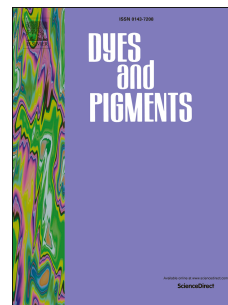


Accepted Manuscript

Host-guest interaction of rotaxane assembly through selective detection of ferric ion: Insight into hemin sensing and switching with sodium ascorbate

Tarun Shukla, Atul Kumar Dwivedi, Reguram Arumugaperumal, Chien-Min Lin, San-Yuan Chen, Hong-Cheu Lin



PII: S0143-7208(16)30118-8

DOI: [10.1016/j.dyepig.2016.03.049](https://doi.org/10.1016/j.dyepig.2016.03.049)

Reference: DYPI 5174

To appear in: *Dyes and Pigments*

Received Date: 15 January 2016

Revised Date: 27 March 2016

Accepted Date: 28 March 2016

Please cite this article as: Shukla T, Dwivedi AK, Arumugaperumal R, Lin C-M, Chen S-Y, Lin H-C, Host-guest interaction of rotaxane assembly through selective detection of ferric ion: Insight into hemin sensing and switching with sodium ascorbate, *Dyes and Pigments* (2016), doi: 10.1016/j.dyepig.2016.03.049.

This is a PDF file of an unedited manuscript that has been accepted for publication. As a service to our customers we are providing this early version of the manuscript. The manuscript will undergo copyediting, typesetting, and review of the resulting proof before it is published in its final form. Please note that during the production process errors may be discovered which could affect the content, and all legal disclaimers that apply to the journal pertain.

Host-Guest Interaction of Rotaxane Assembly through Selective Detection of Ferric Ion: Insight into Hemin Sensing and Switching with Sodium Ascorbate

Tarun Shukla, Atul Kumar Dwivedi, Reguram Arumugaperumal, Chien-Min Lin, San-Yuan Chen, and Hong-Cheu Lin*

Department of Materials Science and Engineering, National Chiao Tung University, Hsinchu, Taiwan

E-mail: linhc@mail.nctu.edu.tw

Abstract:

A mechanically interlocked host rotaxane was synthesized by incorporation of tetraphenylethylene and phenanthroimidazole units in the axle to exhibit significant emission bands and demonstrate host-guest interactions via its topologically constrained cavity, and thus to induce a significant and selective fluorescence quenching of rotaxane towards ferric ion (Fe^{3+}). The quenching efficiencies of rotaxane with both ferric ion (Fe^{3+}) and bio-molecular Hemin (containing ferric ion) were investigated to compare the sensitivities of rotaxane for ferric ion and bio-molecular Hemin. The present study could probe host-guest interactions of rotaxane with ferric ion (Fe^{3+}) and Hemin as well as monitoring the biological conversion of Hemin to Heme in presence of sodium ascorbate (as a reducing agent), where the reduced non-toxic Heme could be generated from the toxic form of Hemin.

Keywords: rotaxane • tetraphenylethylene • aggregation induced emission • host-guest interaction • ferric ion

1. Introduction

Mechanically interlocked architecture molecules with topologically constrained ring structures through non-covalent linkages have attracted much attention from several research groups during last few decades. The excellent molecular recognition of mechanically interlocked systems are significantly offered by various guest and host molecules [1]. Recently, the self-motivated behavior of mechanically interlocked molecules (MIMs) have played a crucial role for vital developments in nanotechnological applications [2], including molecular memory [3], mechanical actuators [4], and drug delivery vehicles [5]. The properties of molecular switches and machines associated with MIMs are pronounced to control the dynamics of MIMs in the presence of external stimuli, which have been well studied and established in recent research [6]. Based on the aforementioned concept, some specific optical (perylene bisimides) [7] or electrochemical (ferrocene) [8-9] receptor groups have been frequently employed. Once incorporated into interlocked molecules, these receptor groups have specific signal transduction properties and prominent selectivities towards sensing guest species [10-12]. Therefore, the design and construction of MIMs with specific groups [13] can provide an excellent platform towards probing the host-guest interactions for specific molecular recognitions [14-19]. Due to external stimuli, MIMs binding with cations are capable of showing different emission colours or intensity changes [20-26]. In addition, host-guest sensors based on fluorometric changes have received much attention due to their potential applications in environmental science, chemistry, biology, and medicine [27-30]. The challenges of developing unique water-soluble structures

have been reported recently based on molecular switches in aqueous solution [31-34], where most biological applications are possible via supramolecular chemistry [35,36].

The photophysical phenomena of luminogenic compounds originated from host-guest complexation and aggregation induced emission (AIE) are non-emissive when soluble in good solvents but become highly emissive as aggregated species in poor, which have been studied and investigated over last decade [37,38]. Many aromatic compounds and dyes have the ability to exhibit AIE including hexaphenylsilole, anthracene, and pyrrole derivatives [39], owing to the restriction of intramolecular motions (RIM). Presently, tetraphenylethylene (TPE) is one of the most favorite units due to its extraordinary AIE behaviour [40-43]. Therefore, several reports have demonstrated the utilization of AIE in a variety of fields, such as chemical sensors [44], stress sensors [45], explosive detections [46], and biosensors [47]. Importantly, a fluorescent sensor based on the phenanthroimidazole (PIZ) unit with a less intense emission in contrast to the aggregated TPE unit has been reported [48]. Therefore, the combination of TPE and PIZ units were finely tuned for fluorescence emissions towards selective analytes.

Herein, the synthesis of rotaxane **R1** incorporated with TPE and PIZ units as axle components was accomplished via the conventional metal template method [49]. Interestingly, the AIE behavior of the designed **R1** was visualized with bright blue emissions in semi-aqueous solutions of DMSO with high water content. However, the emission band from the PIZ unit of **R1** (i.e., no AIE phenomenon) was observed in pure and semi-aqueous (with low water contents) DMSO solutions. Interestingly, the presence of Fe^{3+} ion quenched the fluorescence of both TPE and PIZ chromophoric units in semi-aqueous conditions selectively by means of host-guest interactions into the topologically constrained cavity of **R1**. Moreover, the selectivity of Fe^{3+} in the cavity of

R1 was further visualized as fluorescence quenching with ferric ion containing biomolecular Hemin with an enhanced sensitivity, where the quenching efficiency was measured by the extent of AIE from the TPE as well as the fluorescence of PIZ. However, the fluorescence emission of **R1** in a system with a lower water content was proportionally enhanced in the presence of the antioxidant sodium ascorbate and thus to signify the existence of Heme as a result of conversion of Hemin to Heme [50]. Such a conversion could be probed by the generation of optical events in **R1**. This study represents the first example of significant interactions of a macromolecular rotaxane with cyclic ferriprotoporphyrin IX, along with probing the transformation of Hemin (containing ferric ion Fe^{3+}) into Heme (containing ferrous ion Fe^{2+}) by means of an antioxidant (sodium ascorbate).

2. Experimental Section

2.1 Materials

All reagents and most solvents were purchased from Aldrich Chemicals and used without further purification. Solvents were degassed by freeze/thaw/pump cycle technique, and tetrahydrofuran (THF), chloroform (CHCl_3), dichloromethane (DCM), acetonitrile (MeCN), and *N,N*-dimethylformamide (DMF) were dried prior to use. All reactions were carried out under nitrogen atmosphere. The following compounds, including 2,7-dibromophenanthrene-9,10-dione [49], 3-(2-bromoethoxy)phenol [49], 2,6 bis(bromomethyl)pyridine [51], 4-(1,2,2-triphenylvinyl)phenol [52], and macrocycle Pd-complex (MCC) [52], were prepared according to the literature procedures.

2.2 Characterization

NMR spectra were recorded on Varian Inova 400 and Bruker DRX-300 Avance series (^1H : 300, 400, MHz; ^{13}C : 100 and 75 MHz) at 298 K. The chemical shifts were reported in parts per million (ppm) from low to high fields and referenced to residual solvents (^1H and ^{13}C , CDCl_3 $\delta = 7.26$ ppm and $\delta = 77.23$ ppm; $\text{DMSO-}d_6$ $\delta = 2.49$ ppm and $\delta = 39.56$ ppm, respectively). All values of coupling constant (J) were reported in Hertz (Hz). The standard abbreviations of multiplicities were used as follows: s = singlet, d = doublet, t = triplet, m = multiplet, br = broad. In addition, UV-Vis spectra in different solvents were obtained by a Jasco UV600 spectrophotometer using 1 cm quartz cuvette. Fluorescence measurements were performed with HITACHI 4000 Series Spectrophotometer. PL emission and excitation spectra were collected (slit: 5 nm, 10 nm, PMT voltage: 650 V, 450 V, scan limit: 1200 nm/min) for the detector response and the lamp output. Elemental analyses were conducted on HERAEUS CHN-OS RAPID elemental analyser. High resolution mass spectroscopic (HRMS) measurements were performed using Bruker Daltonics Flex Series ESI mass via a buffer solution of α -cyano-4-hydroxycinnamic acid (CHC). Thin layer chromatographies (chromatographies were performed on Merck silica gel under pressure using TLC) were performed on glass plates coated with silica 60 F24 (Merck). The plates were visualized using ultra-violet light (256 nm) and developed using an iodine chamber.

2.3 Synthesis

{5,10-Dibromo-2-(4-(prop-2-yn-1-yloxy)phenyl)-3a,11b-dihydro-1H-phenanthro[9,10-

d]imidazole} (1): A mixture of 2,7-dibromophenanthrene-9,10-dione (2.0 g, 5.50 mmol), 4-(prop-2-yn-1-yloxy) benzaldehyde (2.2 g, 13.77 mmol), and ammonium acetate (6.36 g, 82.63 mmol) in acetic acid (40 mL) was refluxed overnight. After completion of the reaction, the

reaction mixture was cooled to room temperature and poured into water (500 mL). The resulting precipitate material was filtered, and washed with water and hexane sequentially. The material was dried overnight under vacuum at room temperature. The crude compound was crystallized from ethanol to give the target compound as a colourless solid material (2.6 g, 93%). mp: > 195 °C. $^1\text{H NMR}$ (400 MHz, DMSO- d_6 , 298 K) δ (ppm): 13.30 (s, 1H, NH), 8.64-8.56 (m, 4H, ArH), 8.178 (dd, $J = 8.8$ Hz, 2H), 7.64 (d, $J = 8.8$ Hz, 2H), 7.18 (dd, $J = 8.8$ Hz, 2H), 4.90 (s, 2H), 3.61 (s, 1H). $^{13}\text{C NMR}$ (100 MHz, CDCl₃, 298 K), δ (ppm): 158.7, 150.3, 136.9, 128.2, 126.5, 124.4, 123.6, 121.2, 115.6, 79.4, 78.9, 56.0, 40.5, 40.3, 40.1, 39.9, 39.7, 39.4, 39.2.

{5,10-Dibromo-1-hexyl-2-(4-(prop-2-yn-1-yloxy)phenyl)-3a,11b-dihydro-1H

phenanthro[9,10-*d*]imidazole} (2): To a solution of compound **1** (2.5 g, 4.9 mmol) and K₂CO₃ (2.04 g, 14.82 mmol) in DMF (10 mL), iodohexane (2.19 mL, 14.82 mmol) was added and heated at 70°C. After 6 h, the reaction mixture was poured into ice water (100 mL) and extracted with EtOAc (150 mL). The isolated organic layer was washed with brine (250 mL), and then concentrated under vacuum. Then, the crude residue was subjected to column chromatography (silica gel, EtOAc / hexane: 1/4) to give a colourless solid (2.8 g, 95%). mp: > 180 °C. IR (KBr, cm⁻¹): 3306, 3085, 2976, 2901 (propargyl), 2855, 2141, 1660, 1555, 1400, 1310, 1251, 1115. $^1\text{H NMR}$ (400 MHz, DMSO- d_6 , 298 K) δ (ppm): 8.85 (d, $J = 2.4$ Hz, 1H), 8.41 (d, $J = 6.4$ Hz, 1H), 8.30 (d, $J = 8.8$ Hz, 1H), 8.18 (s, 1H), 7.64 (d, $J = 8.4$ Hz, 2H), 7.61 (t, $J = 8.8$ Hz, 2H), 7.14 (d, $J = 8.4$ Hz, 2H), 4.78 (s, 2H), 4.42 (t, $J = 7.6$ Hz, 2H), 2.58 (s, 1H), 1.87 (t, $J = 7.6$ Hz, 2H), 1.29-1.24 (m, 6H), 0.84 (t, $J = 6.0$ Hz, 3H). $^{13}\text{C NMR}$ (100 MHz, CDCl₃, 298 K) δ (ppm): 158.6, 152.9, 137.4, 131.2, 128.6, 125.1, 124.4, 123.2, 1231.2, 115.2, 78.1, 76.7, 75.9, 55.9, 46.7, 31.0, 30.1, 26.0, 22.4, 13.9. HRMS (ESI) (m/z): [M+H]⁺ calcd for C₃₀H₂₇Br₂N₂O, 589.0485, found: 591.0466.

{3-(2-Azidoethoxy)phenol} (3): To a solution of 3-(2-bromoethoxy)phenol (2.5 g, 11.62 mmol) in DMF (20 mL), the sodium azide (1.51 g, 23.25 mmol) was added and then the reaction mixture was heated at 65°C overnight. After the completion of reaction, the reaction mixture was poured into ice water (100 mL) and extracted with EtOAc (350 mL). The organic layer was dried over MgSO₄ and then the solvent was evaporated under vacuum. The crude residue was purified by column chromatography (silica gel, EtOAc / hexane: 1/1) to afford a transparent oil (1.8 g, 86%). mp: > 60 °C. ¹H NMR (400 MHz, DMSO-*d*₆, 298 K) δ (ppm): 7.13 (t, *J* = 8.0 Hz, 1H), 6.53-6.43 (m, 3H), 4.02(t, *J* = 4.8 Hz, 2H), 3.50 (t, *J* = 5.2 Hz, 2H). ¹³C NMR (100 MHz, CDCl₃, 298 K) δ (ppm): 159.4, 156.9, 130.4, 108.7, 106.8, 102.4, 66.9, 50.0.

{2-((3-(2-Azidoethoxy)phenoxy)methyl)-6-(bromomethyl)pyridine} (4): A mixture of compound **3** (1.5 g, 8.37 mmol), 2,6 bis(bromomethyl)pyridine (2.19 g, 8.37 mmol), and K₂CO₃ (3.4 g, 25.13 mmol) in MeCN (30 mL) were heated at 70 °C to react for 5 h. Then, MeCN was removed by evaporation under vacuum and the crude was purified by column chromatography (silica gel, EtOAc/hexane: 4/1). The desired compound was obtained as a colourless solid (1.25 g, 41%). mp: > 65 °C. ¹H NMR (400 MHz, DMSO-*d*₆, 298K) δ (ppm): 7.17 (t, *J* = 8.0 Hz, 1H), 7.45 (d, *J* = 8.0 Hz, 1H), 7.43 (d, *J* = 8.0 Hz, 1H), 7.19 (t, *J* = 8.0 Hz, 1H), 6.60 (dd, *J* = 10.0 Hz, 1H, *J* = 7.6 Hz, 1H), 6.58 (t, *J* = 2.4 Hz, 1H), 6.54 (dd, *J* = 10.0 Hz, 1H *J* = 8.0 Hz, 1H), 5.17 (s, 2H), 4.57 (s, 2H), 4.11 (t, *J* = 5.2 Hz, 2H), 3.57 (t, *J* = 4.8 Hz, 2H). ¹³C NMR (100 MHz, CDCl₃, 298 K) δ (ppm): 159.5, 159.4, 157.2, 156.2, 137.8, 130.1, 122.3, 120.5, 107.6, 107.4, 101.9, 50.1, 33.6.

{2-((3-(2-Azidoethoxy)phenoxy)methyl)-6-(4-(1,2,2-triphenylvinyl)phenoxy)methyl)pyridine} (5): To a solution of 4-(1,2,2-triphenylvinyl)phenol (0.76 g, 2.20 mmol) and compound **4** (0.80

g, 2.20 mmol) in MeCN (20 mL), K_2CO_3 (1.52 g, 11.04 mmol) was added. The reaction mixture was heated at 70 °C to react overnight. After completion of the reaction, the mixture was filtered and the organic layer was concentrated under vacuum. The crude was purified by column chromatography (silica gel, EtOAc/hexane: 4/1), and the desired compound was obtained as a colourless solid (1.1 g, 79%). mp: > 135 °C. IR (KBr, cm^{-1}): 3115, 3020, 2935, 2865, 2108 (azide), 1598, 1351, 1202. **NMR** (400 MHz, DMSO- d_6 , 298 K) δ (ppm): 7.75 (t, $J = 8.0$ Hz, 1H), 7.45 (q, $J = 7.6$ Hz, 2H), 7.21 (t, $J = 8.0$ Hz, 1H) 7.13-7.01 (m, 15H), 6.973 (d, $J = 6.8$ Hz, 2H), 6.75 (d, $J = 6.8$ Hz, 2H), 6.64 (d, $J = 2.4$ Hz, 1H), 6.61 (q, $J = 4.8$ Hz, 1H), 6.56 (dd, $J = 2.4$ Hz, 1H, $J = 2.0$ Hz, 1H), 5.20 (d, $J = 5.2$ Hz, 2H), 5.13 (s, 2H), 4.13 (t, $J = 4.8$ Hz, 2H), 3.58 (t, $J = 4.8$ Hz, 2H). **^{13}C NMR** (100 MHz, $CDCl_3$, 298 K) δ (ppm): 159.6, 159.4, 156.9, 156.7, 156.6, 143.9, 143.8, 140.3, 136.6, 131.3, 127.6, 126.2, 120.2, 120.1, 114.7, 113.9, 107.6, 107.3, 102.0, 70.5, 70.4, 66.9, 50.1. HRMS (ESI) (m/z): $[M+H]^+$ calcd for $C_{41}H_{35}N_4O_3$, 631.2704, found: 631.2705.

5,10-Dibromo-1-hexyl-2-(4-((1-(2-(3-((6-((4-(1,2,2-triphenylvinyl)phenoxy)methyl)pyridin-2-yl)methoxy)phenoxy)ethyl)-1H-1,2,3-triazol-4-yl)methoxy)phenyl)-1H-phenanthro[9,10-d]imidazole (S1): The solution of compound **2** (0.18 g, 0.30 mmol) and compound **5** (0.20 g, 0.31 mmol) in THF/water (10 mL/5 mL) was degassed with nitrogen for 5 min. Then, $CuSO_4$ (0.057 g, 0.31 mmol) and sodium ascorbate (0.19 g, 0.63 mmol) were added sequentially, and the color change was observed. The reaction mixture was stirred at room temperature for 12 h, then the solution was concentrated from the reaction mixture and diluted with a mixed solvent of CH_2Cl_2 (100 mL) and ammonium hydroxide solution (20 mL). The solution was stirred for 1 h at room temperature, then the organic layer in CH_2Cl_2 was separated and concentrated under vacuum. The desired product was isolated from 1.5% MeOH in DCM as a pale yellow solid

(0.29 g, 75%). mp: > 115 °C. IR (KBr, cm⁻¹): 3132, 3045, 3030, 2958, 2888, 1667, 1552, 1458, 1254, 1458, 1253, 1092. ¹H NMR (400 MHz, DMSO-*d*₆, 298 K) δ (ppm): 8.90 (s, 1H), 8.55 (d, *J* = 8.8 Hz, 1H), 8.41 (d, *J* = 8.8 Hz, 1H), 8.30 (s, 1H), 7.85 (s, 1H), 7.72-7.63 (m, 5H), 7.41 (d, *J* = 7.6 Hz, 2H), 7.26 (s, 1H), 7.19 (d, *J* = 8.8 Hz, 2H), 7.11-6.99 (m, 15H), 6.72 (d, *J* = 8.4 Hz, 2H), 6.61 (d, *J* = 8.4 Hz, 2H), 6.57 (d, *J* = 8.4 Hz, 1H), 6.56 (s, 1H), 6.50 (d, *J* = 8.4 Hz, 1H), 5.32 (s, 2H), 5.15 (d, *J* = 6.4 Hz, 2H), 4.78 (t, *J* = 5.2 Hz, 2H), 4.49 (t, *J* = 7.6 Hz, 2H), 4.36 (t, *J* = 5.2 Hz, 2H), 1.91 (t, *J* = 7.2 Hz, 2H), 1.26 (s, 8H) 0.88-0.82 (m, 3H).

¹³C NMR (100 MHz, CDCl₃, 298 K) δ (ppm): 159.6, 159.3, 158.9, 156.8, 156.7, 156.4, 153.1, 143.9, 143.8, 140.3, 136.6, 128.7, 127.0, 125.5, 123.4, 120.1, 113.9, 107.8, 107.2, 102.1, 70.5, 70.3, 66.2, 62.0, 49.8, 46.8, 31.0, 30.2, 29.6, 29.3, 26.0, 22.6, 22.4, 14.1, 13.9. HRMS (ESI) (m/z): [M+H]⁺ calcd for C₇₁H₆₁Br₂N₆O₄, 1219.3121, found: 1221.3090.

Pseudorotaxane (6): To a solution of macrocycle Pd-complex (**MCC**) (0.811 g, 1.26 mmol) in CHCl₃/MeCN (15/5 mL), compound **5** (0.80 g, 1.26 mmol, 1eq) was added and stirred to react at room temperature for 5 h. The solution was evaporated under reduced pressure and the crude residue was purified by column chromatography (silica gel, 0.5% MeOH in DCM). The desired product was isolated as a yellow solid (0.85 g, 52%). mp: > 170 °C. IR (KBr, cm⁻¹): 3643, 3429, 3207, 3057, 2953, 2108 (azide), 1618, 1361, 1171. ¹H NMR (400 MHz, DMSO-*d*₆, 298 K) δ (ppm): 8.13 (t, *J* = 8.0 Hz, 1H), 7.91 (q, *J* = 14.8 Hz, 4H), 7.63 (d, *J* = 8.0 Hz, 1H), 7.47 (d, *J* = 8.0 Hz, 1H), 7.27 (q, *J* = 11.6 Hz, 2H), 7.15-6.99 (m, 15H), 6.72 (d, *J* = 8.0 Hz, 1H), 6.84 (dd, *J* = 6.4 Hz, 1H, *J* = 2.4 Hz, 1H), 6.62-6.58 (m, 2H), 6.29 (d, *J* = 8.0 Hz, 4H), 6.16 (d, *J* = 8.0 Hz, 4H), 5.37 (s, 2H), 4.66 (d, *J* = 14.4 Hz, 2H), 4.41 (s, 2H), 4.17 (t, *J* = 4.8 Hz, 2H), 3.63-3.38 (m, 18H), 2.03 (m, 2H). ¹³C NMR (100 MHz, CDCl₃, 298 K) δ (ppm): 171.26, 159.4, 158.5, 157.6,

157.3, 155.1, 152.7, 144.0, 143.7, 140.8, 136.9, 131.4, 130.4, 127.5, 125.1, 122.3, 122.2, 114.4, 114.4, 108.1, 107.8, 102.4, 70.69, 69.51, 69.29, 68.0, 67.14, 67.12, 50.13, 49.57. HRMS (ESI) (m/z): [M+H]⁺ calcd for C₇₀H₆₅N₇O₁₀Pd, 1271.5599, found: 1283.5189.

Metalated rotaxane (Pd-complex) (7): A solution of compound **6** (0.50 g, 0.39 mmol) and compound **2** (0.23 g, 0.39 mmol) in THF/H₂O (15 mL/5 mL) was degassed with nitrogen for 5 min, and then CuSO₄ (0.062 g, 0.39 mmol) and sodium ascorbate (0.15 g, 0.786 mmol) were added sequentially to observe the color change. Then, the reaction mixture was stirred at room temperature for 12 h. After this time the solvent was evaporated from the reaction mixture, and the crude was diluted with DCM (100 mL)/ammonium hydroxide solution (20 mL) and stirred for half an hour at room temperature. Then organic layer was isolated and concentrated under vacuum. The crude product was purified by column chromatography (silica gel, 2% MeOH in DCM). The crude product was isolated as a yellow solid (0.56 g) which was used in the next step of the reaction without further purification. mp: > 175 °C. IR (KBr, cm⁻¹): 3078, 3052, 2977, 2917, 2862, 1770, 1675, 1603, 1494, 1397, 1261. HRMS (ESI) (m/z): [M+H]⁺ calcd for C₁₀₀H₉₁Br₂N₉O₁₁Pd, 1858.4312, found: 1860.4327.

Final rotaxane R1: To a solution of crude compound **7** (0.40 g, 0.21 mmol) dissolved in CHCl₃ (10 mL), a solution of KCN (0.21 g, 3.23 mmol) dissolved in MeOH (5 mL) was added. The reaction mixture was stirred at room temperature for 2 h, and then the solvent was evaporated under vacuum. The crude residue was purified by column chromatography (silica gel, 2.5% MeOH in DCM). The desired product was isolated as a colourless solid (0.32 g, 86%). mp: > 120 °C. IR (KBr, cm⁻¹): 3465, 3355, 3075, 3015, 2958, 2842, 1677, 1574, 1495, 1391, 1252, 1102. ¹H NMR (400 MHz, DMSO-*d*₆, 298 K) δ (ppm): 9.28 (t, *J* = 6.0 Hz, 2H), 8.84 (d, *J* = 2 Hz, 1H),

8.55 (d, $J = 9.2$ Hz, 1H), 8.41 (t, $J = 9.2$ Hz, 2H), 8.31 (d, $J = 1.6$ Hz, 1H), 8.00 (t, $J = 8.0$ Hz, 1H), 7.86 (s, 1H), 7.66 (q, $J = 15.2$ Hz, 3H), 7.58 (d, $J = 7.6$ Hz, 2H), 7.25 (d, $J = 7.4$ Hz, 1H), 7.23 (d, $J = 7.8$ Hz, 1H), 7.13-6.98 (m, 19H), 6.89 (d, $J = 8.4$ Hz, 2H), 6.63 (d, $J = 8.0$ Hz, 4H), 6.54 (d, $J = 8.0$ Hz, 2H), 6.45 (t, $J = 10.4$ Hz, 2H), 6.30 (d, $J = 8.0$ Hz, 4H), 6.19 (d, $J = 2.8$ Hz, 1H), 5.03 (s, 2H), 4.78 (s, 2H), 4.57-4.53 (m, 2H), 4.47 (t, $J = 7.6$ Hz, 2H), 4.37 (dd, $J = 6.4$ Hz, 1H, $J = 5.6$ Hz, 1H), 4.29 (dd, $J = 5.6$ Hz, 1H, $J = 6.4$ Hz, 1H), 4.02 (t, $J = 5.6$ Hz, 2H), 3.84 (d, $J = 4.4$ Hz, 2H), 3.73 (d, $J = 3.6$ Hz, 4H), 3.68 (d, $J = 4.8$ Hz, 4H), 3.63-3.60 (m, 4H), 2.25 (d, $J = 7.2$ Hz, 2H), 1.92 (t, $J = 7.6$ Hz, 2H), 1.28-1.25 (m, 8H), 0.87-0.85 (m, 3H). ^{13}C NMR (100 MHz, CDCl_3 , 298 K) δ (ppm): 163.5, 158.9, 155.6, 153.1, 149.1, 143.8, 143.3, 138.6, 136.6, 128.8, 127.5, 125.9, 124.4, 120.3, 114.9, 113.7, 107.6, 106.8, 101.8, 70.7, 69.2, 67.1, 65.6, 61.7, 49.3, 46.9, 42.5, 31.4, 30.2, 29.6, 29.3, 26.0, 22.6, 22.4, 14.1, 13.9. HRMS (ESI) (m/z): $[\text{M}+\text{H}]^+$ calcd for $\text{C}_{100}\text{H}_{94}\text{Br}_2\text{N}_9\text{O}_{11}$, 1754.5440, found: 1756.5599. Anal. Calcd for $\text{C}_{100}\text{H}_{93}\text{Br}_2\text{N}_9\text{O}_{11}$ (%): C, 68.37; H, 5.34; N, 7.18. Found (%): C, 67.85; H, 5.95; N, 6.45.

3. Results and Discussion

Synthetic Strategy and Photo-Physical Properties of Rotaxane (R1).

Herein, we report the synthesis of the target mechanically interlocked rotaxane **R1** based on square planar Pd (II) complex strategy, as shown in Scheme 1. According to our previous report,⁴⁹ the control axle **S1** was synthesized by following Scheme 1(a). With the treatment of TPE azide terminated compound **5** in the presence of 4-(1,2,2-triphenylvinyl)phenol macro-cycle (Pd-complex) MCC, a predominantly self-complexing pseudorotaxane **6** was produced by the replacement of the acetonitrile segment from MCC in chloroform.

Scheme 1

Using a stoppering strategy, Pd-metalated rotaxane **7** was prepared through the well-known click reaction between pseudorotaxane **6** and PIZ alkyne **2**. Subsequently, through the treatment of Pd-metalated rotaxane **7** with potassium cyanide to remove Pd metal, the target rotaxane **R1** was obtained with an excellent yield of 86% as shown in scheme 1 and displayed a good solubility in most organic solvents.

As most of the biological as well as environmental significant analytes are present in water, we were interested in evaluating the AIE phenomena from TPE and the maximum fluorescence emission from PIZ in the presence of various compositions of semi-aqueous solutions (in water and DMSO solvents). HEPES is a zwitterionic buffering agent to control the pH values within 7.2-7.4. Herein, the HEPES buffer solution was used for the UV-vis and PL experiments to maintain the pH value of 7.4. The UV-vis absorption and PL spectra of **R1** (25 μ M) in different semi-aqueous solutions (in water and DMSO solvents), HEPES (pH 7.4, 10 mM) are displayed in Figure 1.

Figure 1

As shown in Figure 1a, the designed rotaxane **R1** (25 μ M) displayed an absorption pattern in DMSO solvent with well resolved absorption bands centered at 266 nm. As illustrated in Figure 1b, the corresponding emission peak of the photoluminescence (PL) spectra in DMSO is centered at 401 nm and is related to PIZ fluorophore. Due to the complete solubility in pure DMSO, **R1** was found to be non-fluorescent and absent of AIE, where **R1** was in the non-aggregated state of TPE with free rotations of conjugated rings about single bonds. DMSO along with various compositions of water were subjected to investigations concerning the significant variations in emission as well as absorption intensities. An unaltered emission related to PIZ

fluorophore was appeared with 10% water without AIE. It was observed that more than 20% of water up to 80% was able to generate a bright blue AIE centered at 470 nm as shown in Figure 1b. Moreover, the PL emission of **R1** (25 μM) related to TPE was found to be 65 times higher than that of PIZ. The absorption pattern in the presence of high percentages of water was found to be broadened and unrelaxed. The hetero-atoms 'N' and 'O' in the topologically constrained cavity of designed interlocked host rotaxane **R1** were proposed to facilitate the host-guest interactions. An analyte of particular interest could be chelated with **R1** through the specific transduction capabilities associated with appended TPE and PIZ groups. We were more interested in investigating the interactions of guests captured by the macrocyclic cavity and the variations of host-guest interactions to affect photophysical properties of **R1** in two solution media, such as (1) with a lower content of water (10%), where AIE from TPE would be ineffective and thus to transduce the photophysical change solely from PIZ. Therefore, the non-aggregated state of **R1** will be dominant and (2) with a higher content of water (80%), where AIE from TPE would be prominent and the transduction could be obtained with a bright blue emission (the aggregated state). Host-guest interactions were subjected to cations as well as anions in our study, due to their efficient perturbation capabilities in the micro-environment of the host probes. Therefore, various alkali as well as transition metal ions, such as Fe^{2+} , Ni^{2+} , Pb^{2+} , Cu^{2+} , Hg^{2+} , Sn^{2+} , Co^{2+} , Zn^{2+} , Cd^{2+} , Mn^{2+} , Mg^{2+} , Ca^{2+} , Se^{2+} , Ru^{3+} , Fe^{3+} , Al^{3+} , Cr^{3+} , and various anions such as F^- , Cl^- , Br^- , I^- , OH^- , SCN^- , HPO_4^{2-} , H_2PO_4^- , and CN^- ions were chosen to study the chelation ability in the cavity of **R1**. Our preliminary investigations were based on the significant changes in the emission of **R1** in the presence of various metal ions. Because fluorescence is considered to be a highly sensitive optical technique towards prominent changes, to probe the detection of lower concentrations of guest analytes with a lower detection limit is required in nano-molar regime.

Figure 2

Primarily, the non-aggregated state of **R1** (25 μM) was derived with a less content (10% vol.) of aqueous solution, HEPES (pH 7.4, 10 mM) in DMSO and thus a solution medium with 9:1 vol. ratio (DMSO:H₂O) was prepared to monitor the host-guest interaction event. **R1** (25 μM) in the aqueous HEPES solution displayed an emission band intensity centered at 401 nm upon excitation at 350 nm. Upon the addition of various metal ions from 0 to 35 μM in **R1**, variations in the PL emission maxima are shown in Figure 2a. The UV-vis. absorption spectra of **R1** (25 μM) revealed the sign of aggregations as the increment (2.5 eq.) of the concentration for Fe³⁺ ion (35 μM) and a developed band (375 nm) of **R1** in Figure 2b is the confirmation of the internal charge transfer mechanism of **R1** with Fe³⁺ ion. The fluorescence emission of **R1** (25 μM) was almost unaffected in the presence of most alkali and transition metal ions Fe²⁺, Ni²⁺, Pb²⁺, Cu²⁺, Hg²⁺, Sn²⁺, Co²⁺, Zn²⁺, Cd²⁺, Mn²⁺, Mg²⁺, Ca²⁺, Se²⁺, Ru³⁺, Fe³⁺, Al³⁺, Cr³⁺ even at their 35 μM concentrations in Figure 2a.

However, the addition of Fe³⁺ from 0-30 μM significantly quenched the fluorescence of **R1** (25 μM). Our observations show significant fluorescence quenching with a huge red shift of (35 nm) in presence of Fe³⁺ ion within the concentration range from 0 to 30 μM , and that was leveled off over concentrations of 25 μM and thus a less intense and highly red-shifted emission band was observed in Figure 2c. Moreover, the fluorescence quenching of **R1** towards Fe³⁺ ion was found to be 30-fold within the investigated concentration range. The decreasing emission band patterns of **R1** (25 μM) in the presence of Fe³⁺ (0-30 μM) were plotted as shown in Figure 2c.

At lower concentrations of Fe³⁺ ion up to 16 μM , the fluorescence quenching behavior of **R1** was found to be linear. While at higher concentrations up to 25 μM , the linearity was lost and

resulted in a nonlinear behaviour, signifying the possibility of a static quenching as shown in the inset of Figure 2c. The efficiency of fluorescence quenching of **R1** in the presence of Fe^{3+} ion, over the linear region was concluded in terms of Stern–Volmer constant and compared.

$$I_0/I = 1 + K_{sv} [Q] \dots\dots\dots (i)$$

In above equation (i), where I_0 and I are fluorescence intensities in the absence and presence of the quencher, respectively, K_{sv} is the Stern–Volmer constant and the value of K_{sv} of an artificial assay indicates the sensitivity of the probe towards the analyte, and $[Q]$ is the quencher concentration. The K_{sv} value for **R1** (25 μM) in the presence of Fe^{3+} ion (35 μM) was found to be $1.39 \times 10^5 \text{ M}^{-1}$. The high K_{sv} value of **R1** towards Fe^{3+} ion further confirmed that **R1** is a selective and sensitive probe for sensing Fe^{3+} ion in a semi-aqueous medium. The corresponding absorption patterns of **R1** (25 μM) in the presence of Fe^{3+} ion (0-35 μM) within the investigated concentration range revealed broadened and unresolved absorption spectra. Comparably, the absorption patterns of **R1** were visualized in the presence of water without metal ions, which signified an aggregated state of **R1**. Interestingly, one broad band centered around 375 nm was observed as shown in Figure 2c, which may be attributed to the charge transfer band in the presence of Fe^{3+} ion.

However, as the control axle **S1** (25 μM) was treated with Fe^{3+} ion (0-35 μM) as shown in Figure 2 (d), the fluorescence quenching patterns of **S1** were similar but smaller than those of **R1**. Furthermore, as shown in Figure S10, **S1** (25 μM) was mixed with macrocycle **MC** (25 μM) in a molar ratio of 1:1 (in contrast to **R1**) and treated with Fe^{3+} (0-75 μM) ion. The combination of **S1** and **MC** prohibited the fluorescence quenching alteration at the higher concentration of Fe^{3+} ion.

These experiments clarified that only **R1** is the most sensitive and selective probe towards Fe^{3+} ion.

Tunable Aggregation of Rotaxane (R1).

The aggregated state of **R1** (25 μM), derived from the high content (80% vol.) of aq., HEPES buffer (pH 7.4, 10 mM), was subjected to monitor the host-guest interaction event. In such a solvent composition, **R1** displayed an AIE band from TPE, centered at 470 nm, upon the excitation at 350 nm as shown in Figure S6 (b). Under these conditions, a bright blue emission from **R1** was clearly visible under UV light due to a high emission as shown in Figure S6 (c). Furthermore, significant changes in AIE were investigated in the presence of various metal ions. The fluorescence emission of **R1** was found to be almost unaffected in the presence of various alkali and transition metal ions even at the concentration of 100 μM as shown in Figure S6 (a). However, a significant fluorescence quenching towards Fe^{3+} ion within a concentration ranging from 0 to 100 μM was observed and the quenching levelled off at 110 μM concentration in Figure S6 (b). The decreasing fluorescence intensity patterns of **R1** (25 μM) in the presence of Fe^{3+} (0-100 μM) were found to be linear at lower concentrations as shown in the inset of Figure S6 (b). However, at higher concentrations of Fe^{3+} ion (4 eq.) the linearity was lost and the plot became nonlinear indicating the possibility of a static type of quenching. The efficiency of the fluorescence quenching of **R1** in the presence of Fe^{3+} ion was determined over the linear region of the plot by generating a Stern–Volmer plot as described earlier. The obtained K_{sv} value was found to be $0.37 \times 10^5 \text{ M}^{-1}$.

Time-Correlated Single Photon Counting (TCSPC) experiment:

The fluorescence quenching mechanism in non-aggregated (10% aq., HEPES pH 7.4, 10 mM buffer) as well as aggregated (80% aq., HEPES pH 7.4, 10 mM buffer) state of **R1** (25 μ M) stages in DMSO with Fe^{3+} (30 μ M and 100 μ M) was confirmed by carrying out the time-correlated single photon counting (TCSPC) experiments with a nanosecond excitation as shown in Figure 3 and S7.

Figure 3**Table 1**

The TCSPC data displayed unmodified biexponential decay patterns of **R1** (25 μ M) in the absence and presence of Fe^{3+} ion in semi-aqueous conditions. As shown in Table 1, the concluded lifetime values for **R1** in the non-aggregated (10% aq.) and aggregated states (80% aq) of **R1** $\{(\tau_1, 1.78 \text{ ns}, 13.23\%), (\tau_2, 0.24 \text{ ns}, 86.77\%)\}$ and $\{(\tau_1, 4.70 \text{ ns}, 48.34\%), (\tau_2, 1.40 \text{ ns}, 51.66\%)\}$, respectively. It was found to be almost unaffected upon the interaction with Fe^{3+} $\{(\tau_1, 0.83 \text{ ns}, 47.97\%), (\tau_2, 0.13 \text{ ns}, 52.03\%)\}$ and $\{(\tau_1, 5.05 \text{ ns}, 41.90\%), (\tau_2, 1.76 \text{ ns}, 58.10\%)\}$, respectively. The unaffected life time values and decay patterns in both cases clearly indicated the occurrence of a static type of quenching, and thus **R1** formed a non-fluorescent ground state and stable complex [**R1**+ Fe^{3+}] under our experimental conditions.

 ^1H NMR Measurements.

The binding mode was also concluded by ^1H NMR titrations of **R1** in acetone- d_6 solvent in the presence of Fe^{3+} ion from 0 to 1.0 eq. as shown in Figure 4. Upon the addition of Fe^{3+} ion with various increasing concentrations in **R1**, amide protons (*) of cavity were found to be shifted

upfield and the pyridyl proton (17,19) of axle shifted downfield. The further gradual addition of Fe^{3+} ion almost diminished the intensity of the proton peak (*). Such an up-field shift of amide protons are attributed to the capture of Fe^{3+} in the cavity and thus to enhance the N-H bond in the amide region. Therefore, the NMR titrations clearly indicated a stoichiometric ratio of 1:1 between **R1** and Fe^{3+} ion for complex [**R1**+ Fe^{3+}].

Figure 4

In addition, as the axle **S1** was treated with Fe^{3+} ion up to 0-1.0 eq. in Figure S1 of the supporting information, no proton shifts were observed. These results revealed that **R1** is responsible for Fe^{3+} ion interaction due to its H-bonded constrained cavity.

Biomolecule (Hemin) Interactions with Rotaxane (R1). Since the sensor selectivity of **R1** towards ferric ion (Fe^{3+}) has been verified in the previous study, both biological species Hemin (containing ferric ion Fe^{3+}) and Heme (containing ferrous ion Fe^{2+}) are introduced to our investigation of potential biological applications. Hemin can be reduced by antioxidant (sodium ascorbate) [53]. Inspired by such quenching phenomena of **R1** in non-aggregated state (10% aq., HEPES pH 7.4, 10 mM buffer) and aggregated state (80% aq., HEPES pH 7.4, 10 mM buffer), we were more interested in the sensing capability of **R1** for real small biomolecule (Hemin) containing ferric ion (Fe^{3+}). Therefore, we further performed the fluorescence quenching experiments in the presence of Hemin in both conditions of low-fluorescent non-aggregated and high-fluorescent aggregated states for **R1** in the solvent media of 10% and 80% water content. The related PL responses of **R1** towards Hemin in non-aggregated and aggregated states are shown in Figures 5 and S8, respectively.

Figure 5

Upon the addition of Hemin (0-13 μM), into non-aggregated **R1** (25 μM) solution (with aq. 10% vol., in DMSO), we found a significant quenching of the initial emission band centered at 401 nm into two emission bands centered at 380 and 439 nm. Figure 5. However, as demonstrated in Figure S8 considerable quenching of the initial emission band of aggregated **R1** (with aq. 80% vol. in DMSO), centered at 470 nm shifted to the emission band centered at 465 nm in the presence of Hemin (0-50 μM). The quenching efficiencies of Hemin in the non- aggregated as well as aggregated states of **R1** were concluded (in terms of Stern-Volmer constant) in terms of K_{sv} values to be $2.80 \times 10^5 \text{ M}^{-1}$ and $0.9 \times 10^5 \text{ M}^{-1}$, respectively. Therefore, the quenching efficiency of **R1** towards Hemin ($K_{sv} = 2.80 \times 10^5 \text{ M}^{-1}$) was found to be superior over that towards Fe^{3+} ion ($K_{sv} = 1.39 \times 10^5 \text{ M}^{-1}$) and thus to signify a higher sensitivity of **R1** towards Hemin.

Time-Correlated Single Photon Counting (TCSPC) experiments. Furthermore, time-correlated single photon counting (TCSPC) spectra of **R1** (25 μM) in the absence and presence of Hemin in 10% aq., HEPES pH 7.4, 10 mM in DMSO are illustrated in Figure 6, which were analyzed to demonstrate a biexponential decay pattern.

Figure 6

Table 2

As shown in Table 2, the lifetime values obtained for **R1** in the absence and presence of Hemin are summarized as $\{(\tau_1, 1.78 \text{ ns}, 13.23\%), (\tau_2, 0.24 \text{ ns}, 86.72\%)\}$ and $\{(\tau_1, 1.31 \text{ ns}, 11.59\%), (\tau_2, 0.22 \text{ ns}, 88.41\%)\}$, respectively. However, the decay patterns of **R1** in the absence and presence of Hemin displayed less overlapped behaviour in contrast to Fe^{3+} ion (see Figure 3), indicating some interactions of **R1** with Hemin. The overlapped behavior of **R1** in the absence and presence

of Fe^{3+} ion suggested that Fe^{3+} ion formed a non-fluorescent ground state and stable complex $[\mathbf{R1}+\text{Fe}^{3+}]$ due to the smaller size of Fe^{3+} ion compared with Hemin.

^1H NMR Measurements.

Interaction of **R1** with Hemin was further investigated by ^1H NMR titrations of **R1** with Hemin in DMSO-d_6 solvent. As shown in Figure 7, when **R1** (1eq.) solution was titrated with various concentrations (0-1.0 eq.) of Hemin, slight upfield shifts for amidic protons (*) inside the cavity of **R1** were noted following a similar trend to that of Fe^{3+} ion revealed in Figure 4. However, smaller upfield shifts of **R1** were observed with the titration of Hemin as compared with Fe^{3+} ion. These results suggested that stronger interactions of **R1** with Fe^{3+} ion were due to the easier capture of Fe^{3+} ion inside the cavity of **R1**, but the weaker cavity interactions of **R1** with Hemin were attributed to the steric hindrance of central metal ion (Fe^{3+}) coordinated with a larger size Hemin. Our preliminary investigations revealed moderate photophysical alterations in **R1** with Hemin and thus to indicate the occurrence of certain interactions.

Figure 7

Since porphyrins of Heme with Fe^{2+} ion are generally planar in their 6-coordinated geometry, 5-coordinated Hemin leads Fe^{3+} ion out of the central hole towards the 5th ligand, exhibiting some perturbation of the porphyrin core. Therefore, we believe that the porphyrin core in Hemin assisted the availability of ferric ion for **R1** cavity. A close proximity of **R1** and Fe^{3+} ion of Hemin have induced some visualized spectroscopic alterations in **R1**. Regardless of no such strong interactions as **R1** complexed with Fe^{3+} ion, the existence of a close proximity of **R1** and ferric ion of Hemin was further verified based on TCSPS data and NMR titration results.

As we notice that the ferric ion (Fe^{3+}) in the active center of Hemin can be converted to another iron metal ion form, i.e., the ferrous ion (Fe^{2+}), leading to the formation of non-toxic Heme, which can be achieved by means of utilizing some biologically significant reducing agents, such as glutathione and sodium ascorbate. Therefore, we further expanded our analysis by incorporating tripeptide glutathione (GSH) and sodium ascorbate in our experiments. Both non-aggregated (10% aq. vol in DMSO) and aggregated (80% aq. vol. in DMSO) states of **R1** (25 μM) as well as Hemin with concentrations of 13 and 50 μM , respectively, were subjected to monitor the interactions with reducing agents under physiological conditions.

Figure 8

According to the previous results, the responses of **R1** towards Hemin in both non-aggregated and aggregated states with different water contents (10% as well 80% of aq. solutions, respectively) were quenched due to the formation of non-fluorescent complex **R1**-Hemin. Moreover, upon the addition of various amounts of sodium ascorbate (0-8 mM) in complex **R1**-Hemin, a significant increase in emission band centered at 475 nm was observed in the non-aggregated state (10% aq. in DMSO) of Fig 8, but the quenched emission band of **R1**-Hemin was unchanged in the aggregated state (80% aq. in DMSO). However, upon the addition of GSH, our experiments did not reveal any significant changes in the quenched emission band of complex **R1**-Hemin in both non-aggregated and aggregated states. Upon the addition of sodium ascorbate in Figure 8, complex **R1**-Hemin demonstrates a gradual increase in the PL intensity centered at 475 nm in the non-aggregated state (10% aq. in DMSO), where the emission enhancement was leveled off (with 50% recovery of initial emission intensity for **R1**) at 7 mM of sodium ascorbate, which was found to be similar to the AIE band position but with less intensity. By

means of biologically significant reducing agents, such as sodium ascorbate, the reduction form of non-toxic Heme could be induced from the toxic form of Hemin.

4. Conclusions

In conclusion, the mechanically interlocked host rotaxane **R1** with terminal groups of TPE and PIZ units was successively constructed through the method of Pd complexation, click reaction, and removal of Pd metal by potassium cyanide. Both TPE and PIZ stopper units were used in rotaxane **R1** to possess aggregation induced emission (AIE) and low controllable fluorescence with different water contents in DMSO, respectively. The emission of rotaxane **R1** by PIZ as well as TPE both exhibited significant signal quenching through the interaction of Fe^{3+} in the cavity of **R1**, and thus the host-guest interactions of both non-aggregated and aggregated states of **R1** were verified. Moreover, the interactions of **R1** towards Fe^{3+} ion in both semi-aqueous states resulted in a static type of quenching and a non-fluorescent ground state of complex [**R1**+ Fe^{3+}], as defined by the Time-Resolved Photoluminescence (TRPL) studies. In addition, the NMR titrations also indicated a stoichiometric ratio of 1:1 between **R1** and Fe^{3+} ion for complex [**R1**+ Fe^{3+}]. The quenching efficiency of **R1** towards Hemin was found to be superior over that towards Fe^{3+} ion and thus to signify a higher sensitivity of **R1** towards Hemin. The variations of PL emission intensities observed from PIZ in the **R1** (10% aq. in DMSO) could be finely tuned in the presence of the biological reducing agent (i.e., sodium ascorbate), where the enhancement of the red-shifted emission band indicated the formation of Heme from Hemin. Finally, the reduced form of non-toxic Heme could be produced from the toxic form, Hemin, by means of biologically significant reducing agents.

Acknowledgement

Financial support of this project was provided by the Ministry of Science and Technology (MOST) through MOST 103- 2113-M-009-018-MY3.

References

- [1] Fang L, Olson MA, Benítez D, Tkatchouk E, Goddard III WA, Stoddart JF. Mechanically bonded macromolecules. *Chem Soc Rev* 2010;39:17–29.
- [2] Ma X, Tian H. Bright functional rotaxanes. *Chem Soc Rev* 2010;39:70–80.
- [3] Zhang W, DeIonno E, Dichtel WR, Fang L, Trabolsi A, Olsen J-C, Benítez D, Heath JR, Stoddart JF. A solid-state switch containing an electrochemically switchable bistable poly[n] rotaxane. *J Mater Chem* 2011;21:1487–95.
- [4] Browne WR, Feringa BL. Making molecular machines work. *Nat Nanotechnol* 2006;1:25–35.
- [5] Coti KK, Belowich ME, Liong M, Ambrogio MW, Lau YA, Khatib HA, Zink JI, Khashab NM, Stoddart JF. Mechanised nanoparticles for drug delivery. *Nanoscale* 2009;1:16–39.
- [6] Dongen SFMV, Cantekin S, Elemans JAW, Nolte RJM. Functional interlocked systems. *Chem Soc Rev* 2014;43:99–122.
- [7] Li H, Li X, Cao Z-Q, Qu D-H, Ågren H, Tian H. A switchable bis-branched [1]rotaxane featuring dual-mode molecular motions and tunable molecular aggregation. *ACS Appl Mater Interfaces* 2014;6:18921–29.
- [8] Li H, Zhang H, Zhang Q, Zhang Q-W, Qu D-H. A switchable ferrocene-based [1]rotaxane with an electrochemical signal output. *Org Lett* 2012;14:5900–903.

- [9] Liu L, Wang Q, Chang, M, Hu X-Y, Jiang J, Wang L. A ferrocene-functionalized bistable [2] rotaxane with switchable fluorescence. *Asian J Org Chem* 2015;4:221–5.
- [10] Langton MJ, Beer PD. Rotaxane and catenane host structures for sensing charged guest species. *Acc Chem Res* 2014;47:1935–49.
- [11] Lee H, Kim EJ, Ahn J, Noh TH, Jung O-S. Anion effects on formation of metallacyclodimeric silver(I) complexes as a solvent reservoir. *J Mol Struct* 2012;1010:111–5.
- [12] Arumugaperumal R, Srinivasadesikan V, Raju MVR, Lin M-C, Shukla T, Singh R, Lin H-C, Acid/Base and H_2PO_4^- controllable high-contrast optical molecular switches with a novel BODIPY functionalized [2]rotaxane. *ACS Appl Mater Interfaces* 2015;7:26491–503.
- [13] Suzuki Y, Osakada K. Formation, dynamic behavior, and chemical transformation of Pt complexes with a rotaxane-like structure. *Chem Asian J* 2006;1:331–43.
- [14] Caballero A, Zapata F, Beer PD. Interlocked host molecule for anion recognition and sensing. *Coord Chem Rev* 2013;257:2434–55.
- [15] Rebilly J-N, Hessani A, Colasson B, Reinaud O. A versatile strategy for appending a single functional group to a multifunctional host through host–guest covalent-capture. *Org Biomol Chem* 2014;12:7780–5.
- [16] Chen Y-J, Yang S-C, Tsai C-C, Chang K-C, Chuang W-H, Chu W-L, Kovalev V, Chung W-S. Anthryl-1,2,4-oxadiazole-substituted calix[4]arenes as highly selective fluorescent chemodosimeters for Fe^{3+} . *Chem Asian J* 2015;10:1025–34.

- [17] Kim EJ, Ahn J, Lee H, Noh TH, Jung, O-S. Synthesis, structures, and ligating ability of 4-tert-butyl calix[n]arene (iso) nicotinoylate. *Tetrahedron Lett* 2012;53:1240–4.
- [18] Lee H, Noh TH, Jung O-S. A ball-joint-type host–guest system that consists of conglomerate helical metallacyclophanes. *Angew Chem Int Ed* 2013;52:11790–5.
- [19] Suzaki Y, Taira T, Osakada K, Physical gels based on supramolecular gelators, including host–guest complexes and pseudorotaxanes. *J Mater Chem* 2011;21:930–8.
- [20] Ajayaghosh A. Chemistry of squaraine-derived materials: Near-IR dyes, low band gap systems, and cation sensors. *Acc Chem Res* 2005;38:449–59.
- [21] Lee S, Yuen KKY, Jolliffe KA, Yoon J. Fluorescent and colorimetric chemosensors for pyrophosphate. *Chem Soc Rev* 2015;44:1749–62.
- [22] Lee HN, Xu Z, Kim SK, Swamy KMK, Kim Y, Kim S-J, Yoon J. Pyrophosphate-selective fluorescent chemosensor at physiological pH: Formation of a unique excimer upon addition of pyrophosphate. *J Am Chem Soc* 2007;129:3828–29.
- [23] Lee M, Jo S, Lee D, Xu Z, Yoon J. A new naphthalimide derivative as a selective fluorescent and colorimetric sensor for fluoride, cyanide and CO₂. *Dyes Pigm* 2015;120:288–92.
- [24] Song NR, Moon JH, Choi J, Jun EJ, Kim Y, Kim S-J, Lee JY, Yoon J. Cyclic benzobisimidazolium derivative for the selective fluorescent recognition of HSO₄⁻ via a combination of C-H hydrogen bonds and charge interactions. *Chem Sci* 2013;4:1765–71.

- [25] Colasson B, Save M, Milko P, Roithová J, Schröder D, Reinaud O. A ditopic calix[6]arene ligand with N-methylimidazole and 1,2,3-triazole substituents: Synthesis and coordination with Zn(II) cations. *Org Lett* 2007;9:4987–90.
- [26] Hu Y, Liu Y, Kim G, Jun EJ, Swamy KMK, Kim Y, Kim SJ, Yoon J. Pyrene based fluorescent probes for detecting endogenous zinc ions in live cells. *Dyes Pigm* 2015;113:372–7.
- [27] Lakowicz JR. *Topics in fluorescence spectroscopy: Probe design and chemical sensing*, Vol. 4; Plenum Press; New York;1994.
- [28] Park S, Kim W, Swamy KMK, Lee HY, Jung JY, Kim G, Kim Y, Kim S-J, Yoon J. Rhodamine hydrazone derivatives bearing thiophene group as fluorescent chemosensors for Hg²⁺. *Dyes Pigm* 2013;99:323–8.
- [29] Poul NL, Mest YL, Jabin I, Reinaud O. Supramolecular modeling of mono-copper enzyme active sites with calix[6]arene-based funnel complexes. *Acc Chem Res* 2015;48:2097–106.
- [30] Zhang R, Yuan Y, Liang J, Kwok RTK, Zhu Q, Feng G, Geng J, Tang BZ, Liu B. Fluorogen–peptide conjugates with tunable aggregation-induced emission characteristics for bioprobe design. *ACS Appl Mater Interfaces* 2014;6:14302–10.
- [31] Grunder S, McGrier PL, Whalley AC, Boyle MM, Stern C, Stoddart JF. A water-soluble pH-triggered molecular switch. *J Am Chem Soc* 2013;135:17691–94.
- [32] Maurin A, Varatharajan S, Colasson B, Reinaud O. A water-soluble calix[4]arene-based ligand for the selective linear coordination and stabilization of copper(I) ion in aerobic conditions. *Org Lett* 2014;16:5426–29.

- [33] Li H, Fahrenbach AC, Coskun A, Zhu Z, Zhao Y, Botros YY, Sauvage JP, Stoddart JF. A light-stimulated molecular switch driven by radical–radical interactions in water. *Angew Chem Int Ed* 2011;50:6782–88.
- [34] Fang L, Basu S, Sue CH, Fahrenbach AC, Stoddart JF. Syntheses and dynamics of donor-acceptor [2] catenanes in water. *J Am Chem Soc* 2011;133:396–9.
- [35] Coskun A, Spruell JM, Barin G, Dichtel WR, Flood AH, Botros YY, Stoddart JF. High hopes: Can molecular electronics realise its potential? *Chem Soc Rev* 2012;41:4827–59.
- [36] Coskun A, Banaszak M, Astumian RD, Stoddart JF, Grzybowski BA. Great expectations: can artificial molecular machines deliver on their promise? *Chem Soc Rev* 2012;41:19–30.
- [37] Hong Y, Lam JWY, Tang BZ. Aggregation-induced emission. *Chem Soc Rev* 2011;40:5361–88.
- [38] Lee H, Noh TH, Jung O-S. Halogen effects on photoluminescence and catalytic properties: a series of spatially arranged trimetallic zinc(II) complexes. *Dalton Trans* 2014;43:3842–49.
- [39] Liu J, Xu Y, Li X, Tian H. Synthesis and characteristics of a novel pseudorotaxane with the diarylethene as the functional stopper. *Dyes Pigm* 2008;76:294–8.
- [40] Luo J, Xie Z, Lam JWY, Cheng L, Qiu C, Kwok HS, Zhan X, Liu D, Zhu D, Tang BZ. Aggregation-induced emission of 1-Methyl-1,2,3,4,5-Pentaphenylsilole. *Chem Commun* 2001;18:1740–1.

- [41] Liang G, Lam JWY, Qin W, Li J, Tang BZ. Molecular luminogens based on restriction of intramolecular motions through host–guest inclusion for cell imaging. *Chem Commun* 2014;50:1725–27.
- [42] Zhao Z, Deng C, Chen S, Lam JWY, Qin W, Lu P, Wang Z, Kwok HS, Ma Y, Qiu H, Tang BZ. Full emission color tuning in luminogens constructed from tetraphenylethene, benzo-2,1,3-thiadiazole and thiophene building blocks. *Chem Commun* 2011;47:8847–49.
- [43] Upamali KAN, Estrada LA, Neckers DC. Selective detection of Cr(VI) in aqueous media by carbazole-based fluorescent organic microcrystals. *Anal Methods* 2011;3:2469–71.
- [44] Wei T, Zhang P, Shi B, Chen P, Lin Q, Liu J, Zhang Y. A highly selective chemosensor for colorimetric detection of Fe^{3+} and fluorescence turn-on response of Zn^{2+} . *Dyes Pigm* 2013;97:297–02.
- [45] Zhang X, Chi Z, Li H, Xu B, Li X, Zhou W, Liu S, Zhang Y, Xu J. Piezofluorochromism of an aggregation-induced emission compound derived from tetraphenylethylene. *Chem Asian J* 2011;6:808–11.
- [46] Wang J, Mei J, Yuan WZ, Lu P, Qin A, Sun J, Ma Y, Tang BZ. Hyperbranched polytriazoles with high molecular compressibility: Aggregation-induced emission and superamplified explosive detection. *J Mater Chem* 2011;21:4056–59.
- [47] Zhou J, He B, Chen B, Lu P, Sung HHY, Williams ID, Qin A, Qiu H, Zhao Z, Tang BZ. Deep blue fluorescent 2,5-bis(phenylsilyl)-substituted 3,4- diphenylsiloles: Synthesis, structure and aggregation-induced emission. *Dyes Pigm* 2013;99:520–5.

- [48] Lin WL, Cao LZ, Feng J. A cell-permeable fluorescent prochelator responds to hydrogen peroxide and metal ions by decreasing fluorescence. *Anal Chim Acta* 2009;634:262–6.
- [49] Raju MVR, Lin H-C. A novel diketopyrrolopyrrole (DPP)-based [2]rotaxane for highly selective optical sensing of fluoride. *Org Lett* 2013;15:1274–77.
- [50] Dwivedi AK, Saikia G, Iyer PK. Aqueous polyfluorene probe for the detection and estimation of Fe^{3+} and inorganic phosphate in blood serum. *J Mater Chem* 2011;21:2502–07.
- [51] Satapathy R, Wu Y-H, Lin H-C. Novel thieno-imidazole based probe for colorimetric detection of Hg^{2+} and fluorescence turn-on response of Zn^{2+} . *Org Lett* 2012;14:2564–67.
- [52] Raju MVR, Lin H-C. Self-assembly of tetraphenylethene-based [2]catenane driven by acid–base-controllable molecular switching and its enabled aggregation-induced emission. *Org Lett* 2014;16:5564–67.
- [53] Zhang X, Sato M, Sasahara M, Migita CT, Yoshida T. Unique features of recombinant heme oxygenase of *Drosophila melanogaster* compared with those of other heme oxygenases studied. *Eur J Biochem* 2004;271:1713–1724.

Schemes and List of Figures

Scheme 1. (a) Synthesis route of stopper **S1** and (b) final target rotaxane **R1**.

Figure 1. (a) UV-vis absorption and (b) PL spectra of **R1** (25 μM) in 10% aq. solution, and 80% aq. solution, HEPES (pH 7.4, 10 mM) in DMSO.

Figure 2. (a) Bar diagram depicting PL quenching of **R1** in 10% aq., HEPES (pH 7.4, 10 mM) in DMSO with various metal ions. (b) UV spectra and (c) PL spectra of **R1** in above solution with increasing concentration of Fe^{3+} metal ion. (d) Color changes of **R1** visible light and under UV light in above solution. (e) PL spectra of **S1** in above solution with increasing concentration of Fe^{3+} metal ion.

Figure 3. Decay patterns of **R1** in the absence and presence of Fe^{3+} ion in 10% aq., HEPES (pH 7.4, 10 mM) in DMSO.

Figure 4. ^1H NMR titrations of **R1** in acetone- d_6 upon the addition of 0-1.0 eq. Fe^{3+} ion concentration.

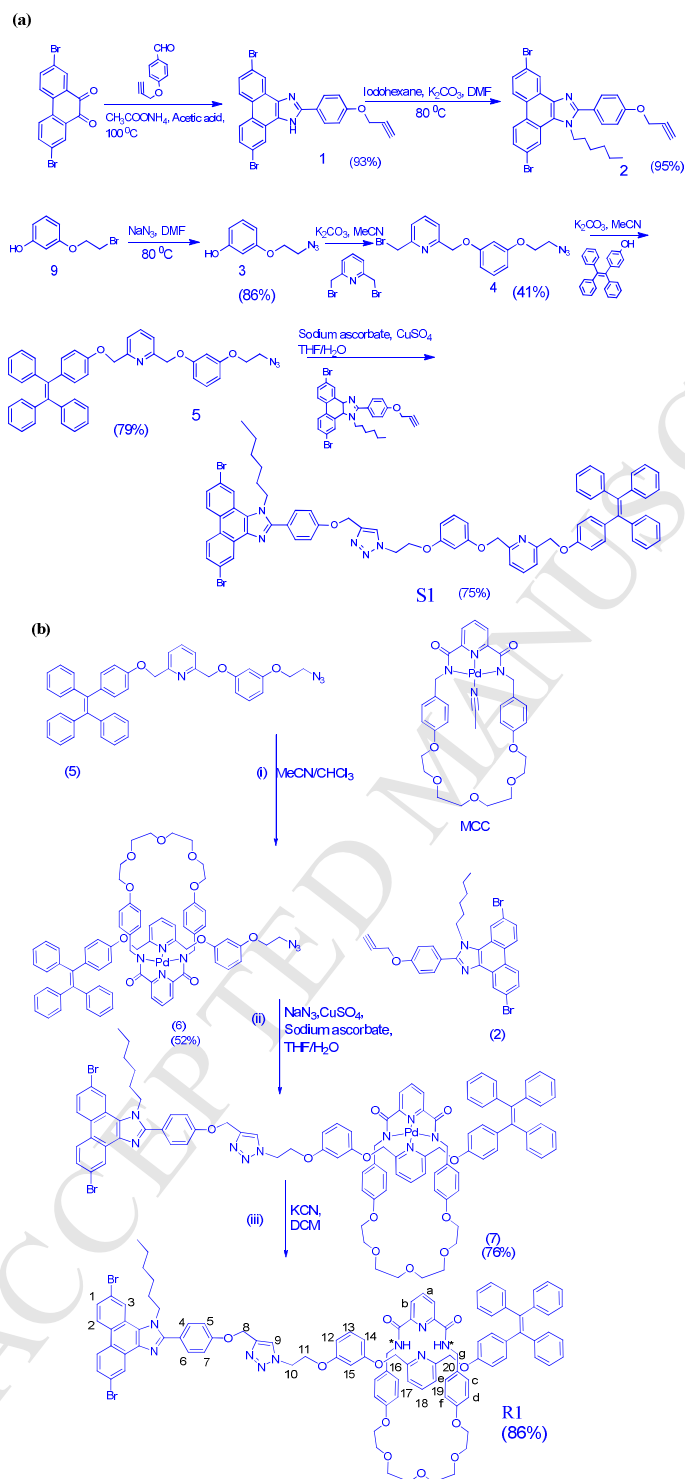
Figure 5. PL titration spectra of **R1** in the presence of Hemin in 10% aq., HEPES (pH 7.4, 10 mM) in DMSO.

Figure 6. Decay patterns of **R1** in the absence and presence of Hemin in 10% aq., HEPES (pH 7.4, 10 mM) in DMSO.

Figure 7. ^1H NMR titrations of **R1** in DMSO- d_6 upon the addition of 0-1.0 eq. Hemin concentration.

Figure 8. PL spectral changes of **R1**+Hemin in the presence of sodium ascorbate in 10% aq., HEPES (pH 7.4, 10 mM) in DMSO.

ACCEPTED MANUSCRIPT



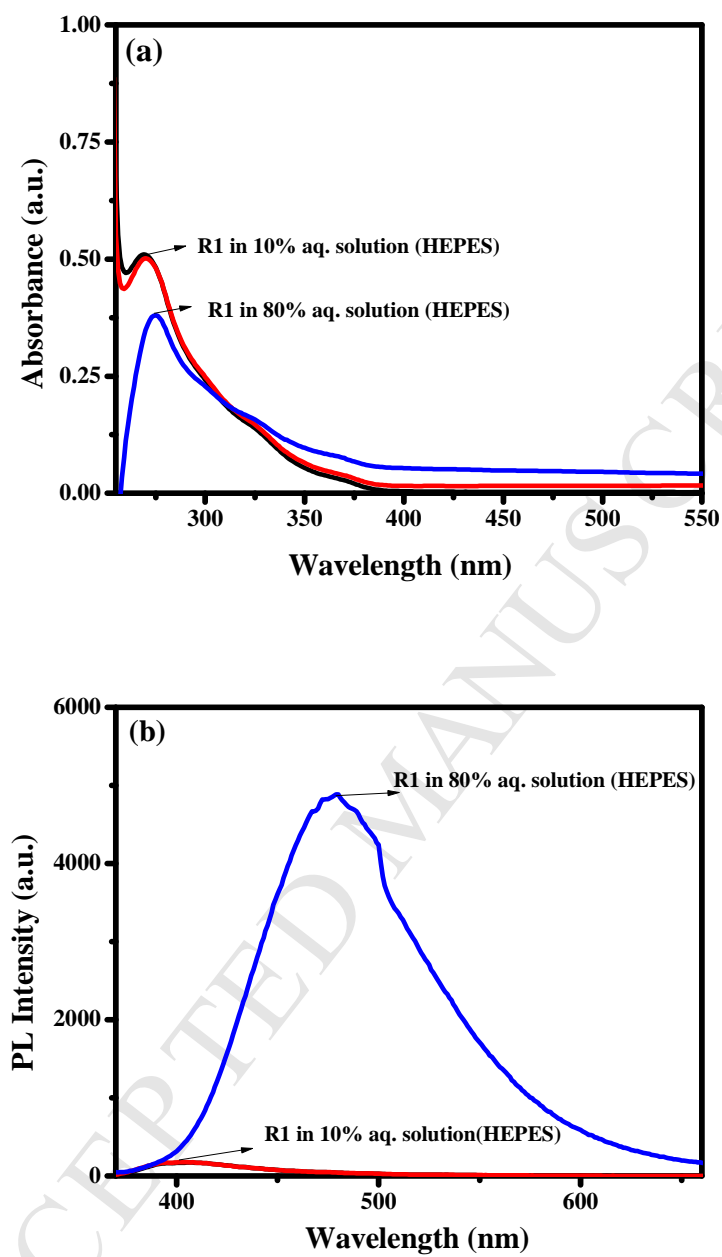


Figure 1. (a) UV-vis absorption and (b) PL spectra of **R1** (25 μM) in 10% aq. solution, and 80% aq. solution, HEPES (pH 7.4, 10 mM) in DMSO.

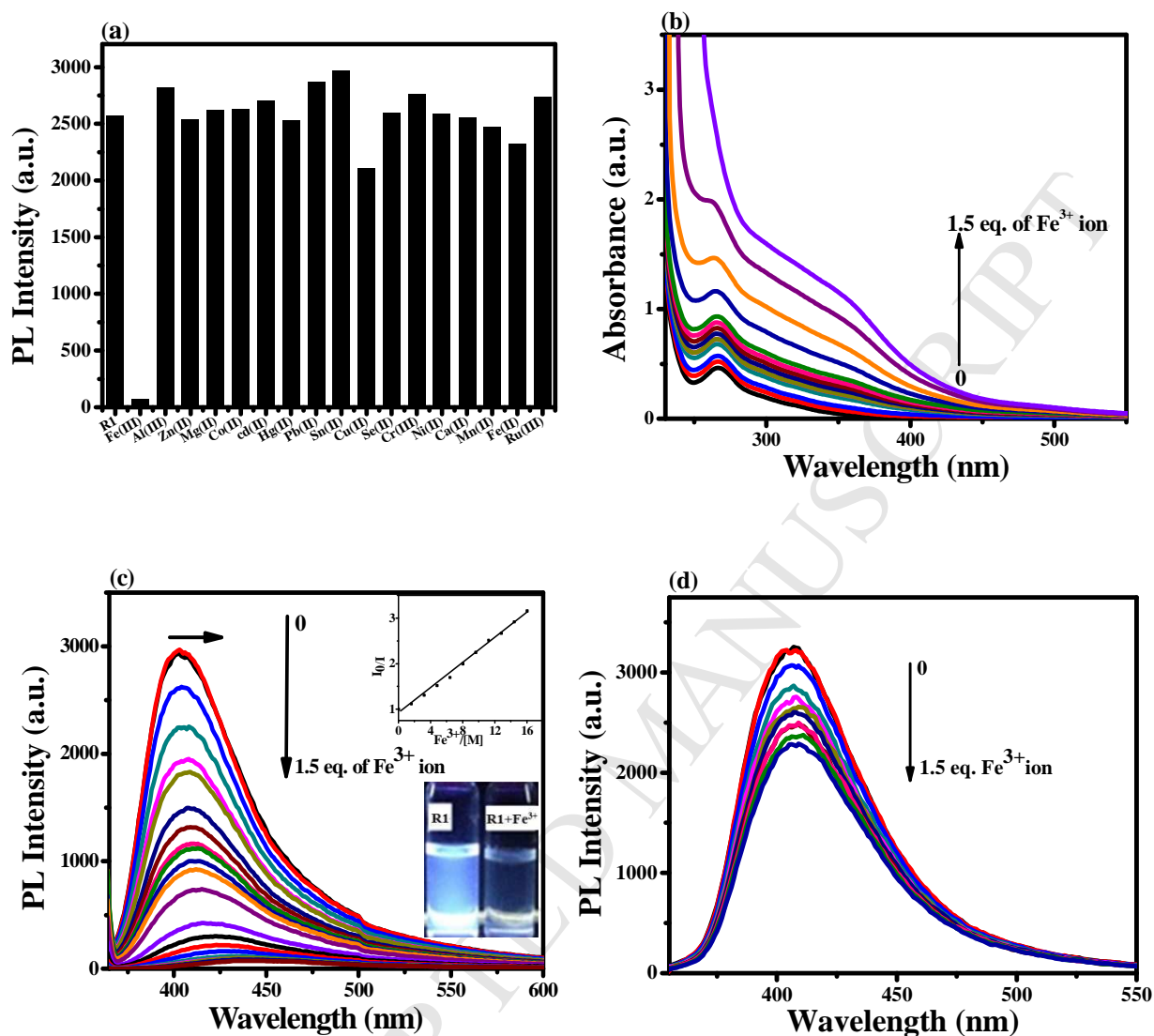


Figure 2 (a) Bar diagram depicting PL quenching of **R1** in 10% aq., HEPES (pH 7.4, 10 mM) in DMSO with various metal ions. (b) UV spectra and (c) PL spectra of **R1** in above solution with increasing concentration of Fe³⁺ metal ion. (Inset color changes of **R1** under UV light in above solution) (d) PL spectra of **S1** in above solution with increasing concentration of Fe³⁺ metal ion.

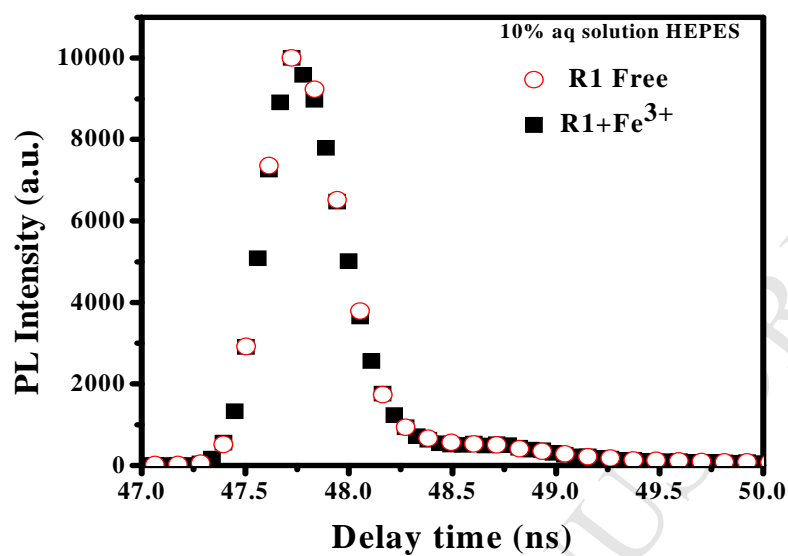


Figure 3. Decay patterns of **R1** in the absence and presence of Fe^{3+} ion in 10% aq., HEPES (pH 7.4, 10 mM) in DMSO.

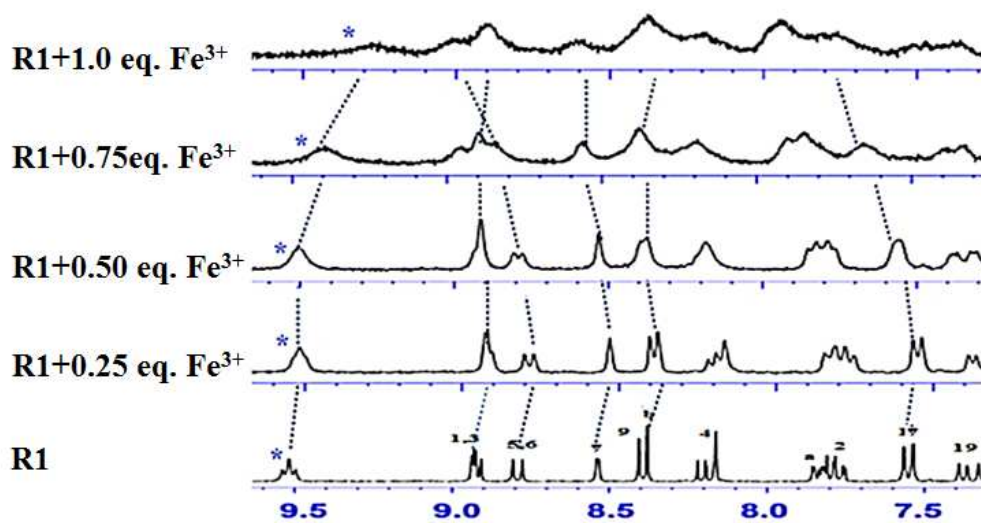


Figure 4 ^1H NMR titrations of **R1** in acetone- d_6 upon addition of 0-1.0 eq. Fe^{3+} ion concentration.

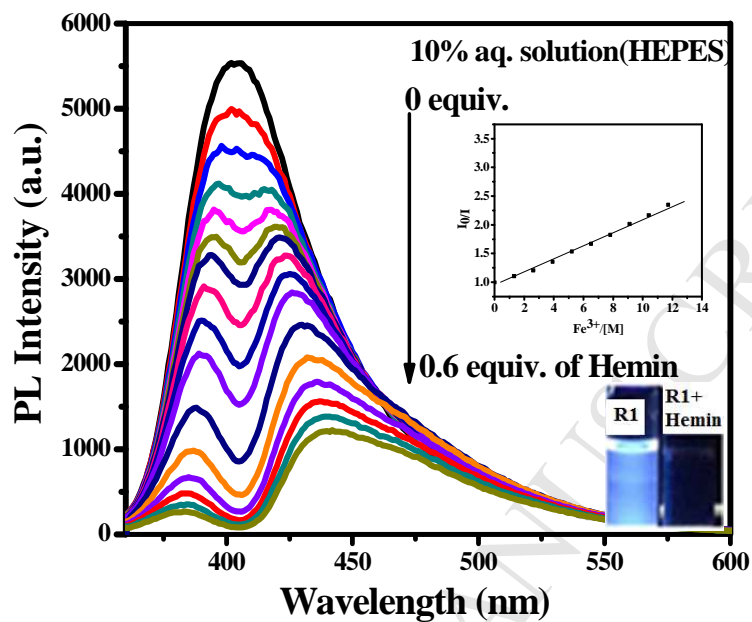


Figure 5 PL titration spectra of **R1** in the presence of Hemin in 10% aq., HEPES (pH 7.4, 10 mM) in DMSO.

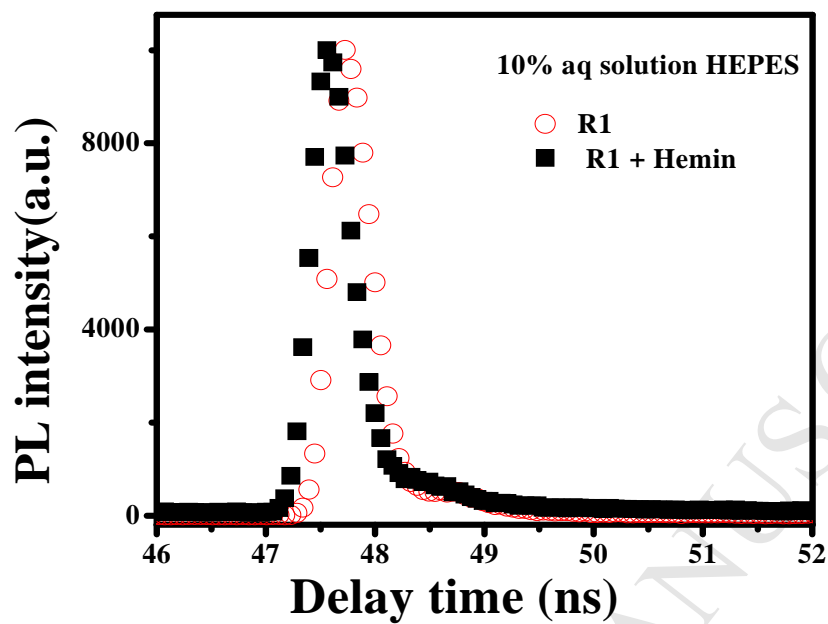


Figure 6 Decay patterns of R1 in the absence and presence of Hemin in 10% aq., HEPES (pH 7.4, 10 mM) in DMSO.

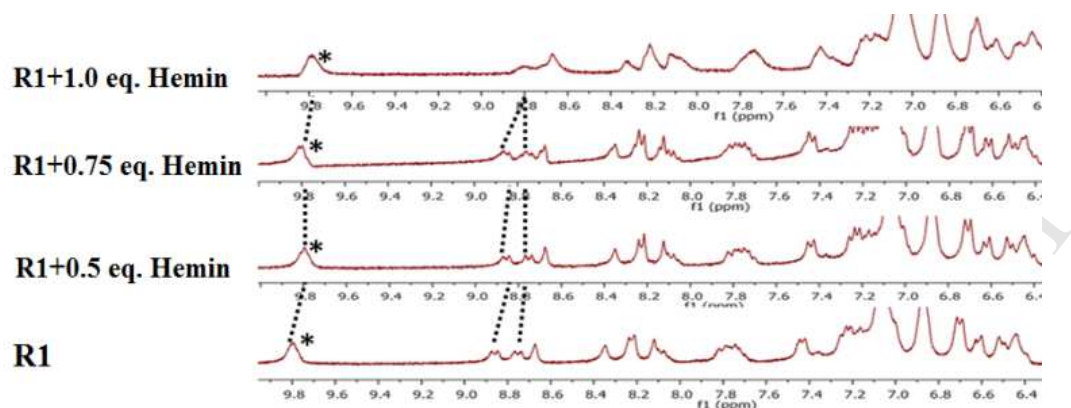


Figure 7 ¹H NMR titrations of **R1** in DMSO-d₆ upon the addition of 0-1.0 eq. Hemin concentration.

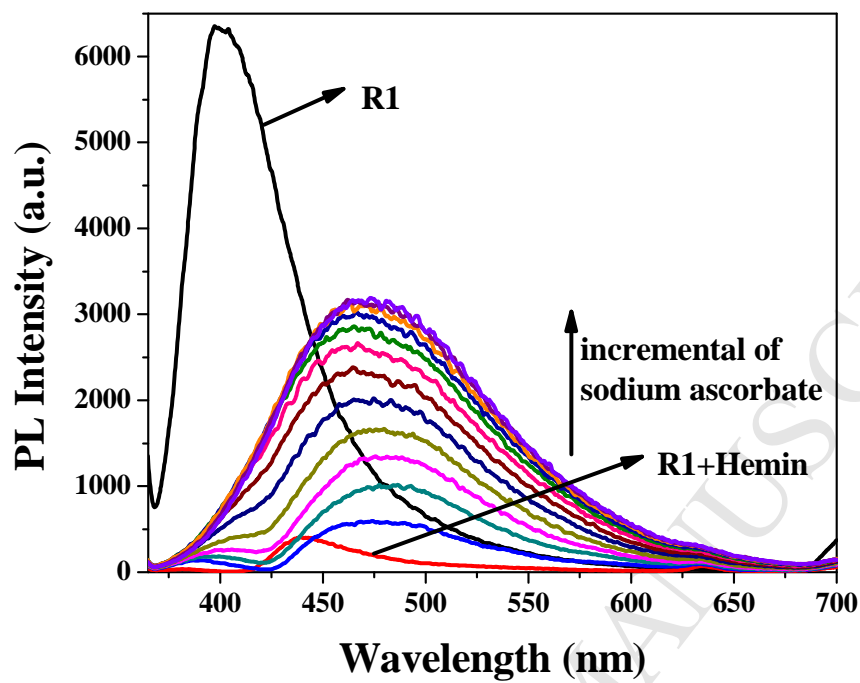


Figure 8 PL spectral changes of **R1+Hemin** in the presence of sodium ascorbate in 10% aq., HEPES (pH 7.4, 10 mM) in DMSO.

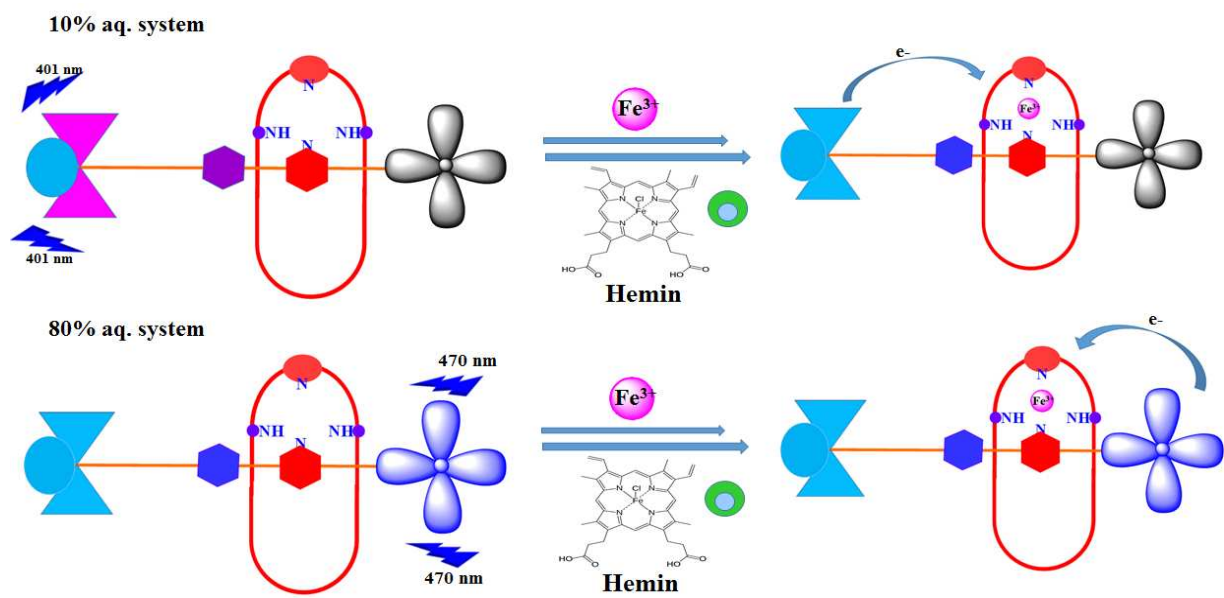
Table 1. Time-resolved fluorescence decay constant (τ) values of **R1** in the presence of Fe^{3+} ion in 10% aq., and 80% aq. HEPES (pH 7.4, 10 mM) in DMSO.

τ (ns)	R1 (10 % aq.)	R1 (10 % aq.) + Fe^{3+}	R1 (80 % aq.)	R1 (80 % aq.) + Fe^{3+}
τ_1	1.78 ns	0.83 ns	4.70 ns	5.05 ns
τ_1 %	13.23 %	47.97 %	48.34 %	41.90 %
τ_2	0.24 ns	0.13 ns	1.40 ns	1.76 ns
τ_2 %	86.72 %	57.03 %	51.66 %	58.10 %

Table 2. Time-resolved fluorescence decay constant (τ) values of **R1** in the presence of Hemin in 10% aq., HEPES (pH 7.4, 10 mM) in DMSO.

τ (ns)	R1 (10% aq.)	R1 (10% aq.) + Hemin
τ_1	1.78 ns	1.31 ns
τ_1 %	13.23 %	11.59 %
τ_2	0.24 ns	0.22 ns
τ_2 %	86.72 %	88.41 %

Graphical Abstract:



Highlights

- This rotaxane is selective and sensitive for Fe^{3+} and Hemin in semi-aq. media.
- The interaction of the synthesized rotaxane towards Hemin is superior to Fe^{3+} ion.
- Transformation of Hemin into Heme is also probed by their interactions with rotaxane.

Supporting Information

Host-Guest Interaction of Rotaxane Assembly through Selective Detection of Ferric Ion: Insight into Hemin Sensing and Switching with Sodium Ascorbate

Tarun Shukla, Atul Kumar Dwivedi, Reguram Arumugaperumal, Chien-Min Lin, San-Yuan Chen, and Hong-Cheu Lin*

Hong-Cheu Lin

Department of Materials Science and Engineering, National Chiao Tung University,

Hsinchu 30049, Taiwan

linhc@mail.nctu.edu.tw

Content

1. Mass chromatograms (HRMS)	02-07
2. 2D ^1H - ^1H COSY NMR.....	08
3. Supporting figures	09-19
4. (^1H and ^{13}C)NMR spectral data	20-28

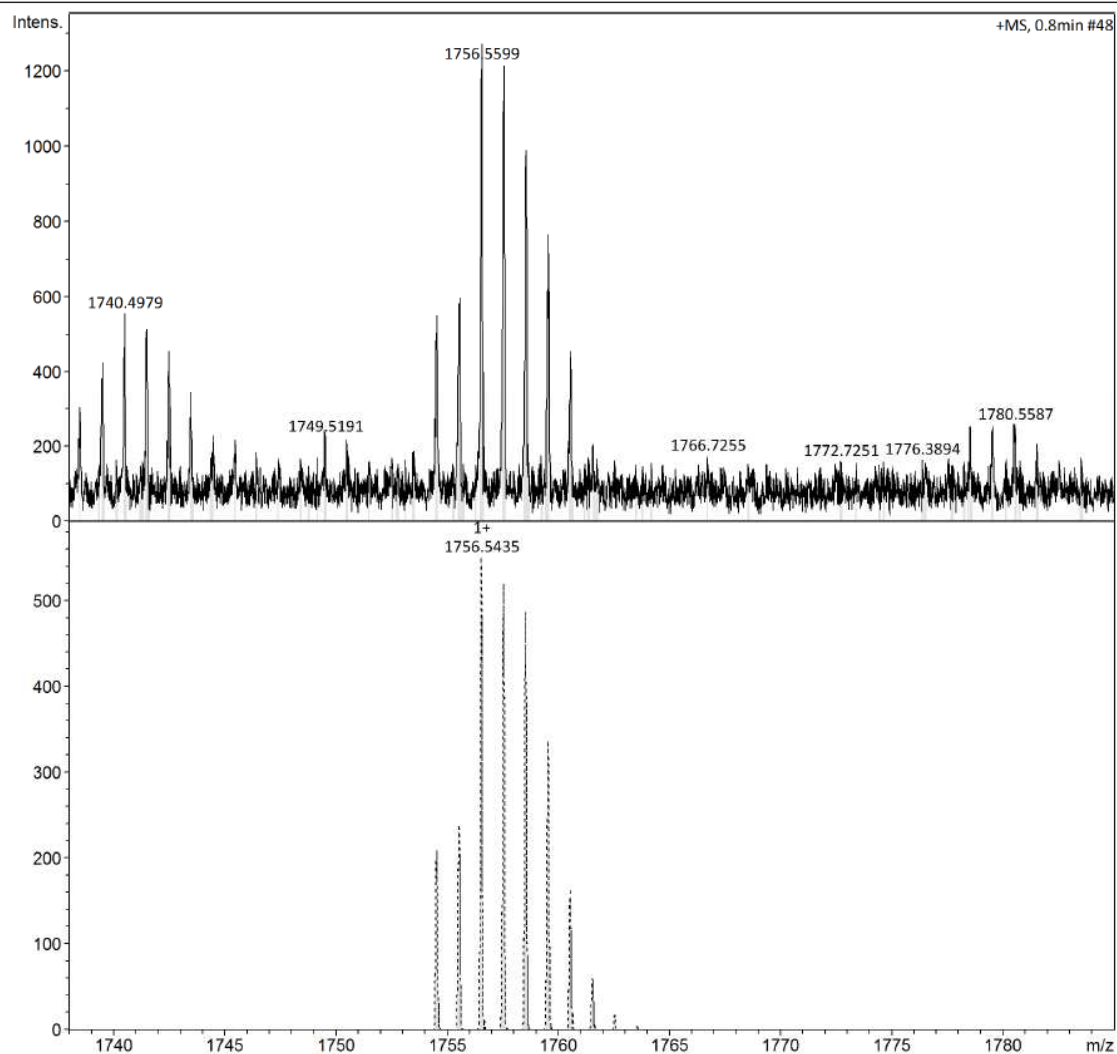
1. HRMS spectra of R1

Analysis Info

Analysis Name D:\Data\NCTU SERVICE\Data\20140326\R-1 1753_GA2_01_898.d Acquisition Date 3/26/2014 4:00:41 PM
Method MW600-3000.m Operator NCTU
Sample Name R-1 1753 Instrument impact HD 1819696.00164
Comment

Acquisition Parameter

Source Type	ESI	Ion Polarity	Positive	Set Nebulizer	1.0 Bar
Focus	Active	Set Capillary	4500 V	Set Dry Heater	200 °C
Scan Begin	50 m/z	Set End Plate Offset	-500 V	Set Dry Gas	6.0 l/min
Scan End	3000 m/z	Set Charging Voltage	2000 V	Set Divert Valve	Waste
		Set Corona	0 nA	Set APCI Heater	0 °C



HRMS spectra of axle S1

Analysis Info

Analysis Name D:\Data\NCTU SERVICE\Data\20140326\S-1 1218_GA3_01_899.d
Method MW600-3000.m
Sample Name S-1 1218
Comment

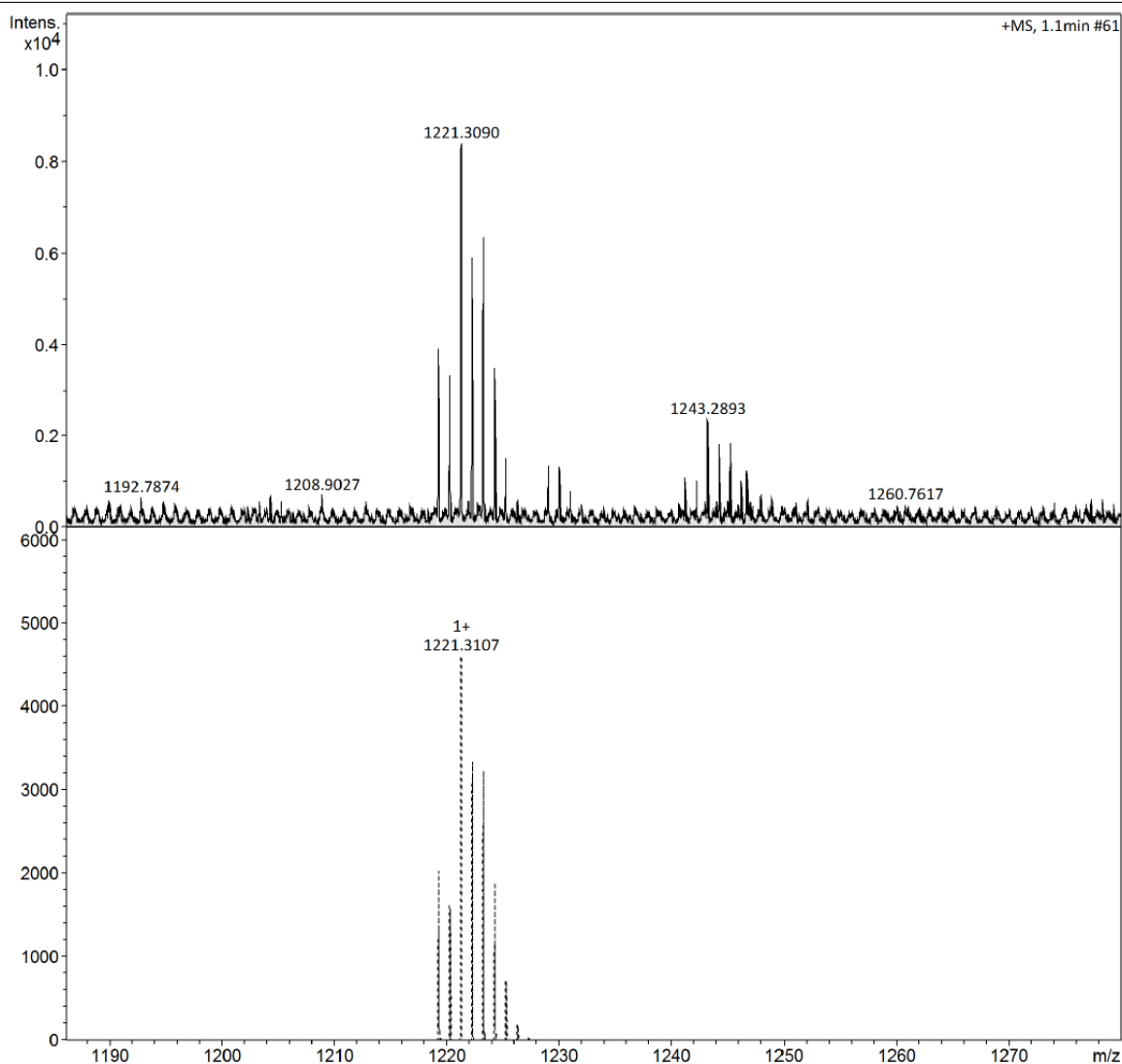
Acquisition Date 3/26/2014 4:05:00 PM

Operator NCTU

Instrument impact HD 1819696.00164

Acquisition Parameter

Source Type	ESI	Ion Polarity	Positive	Set Nebulizer	1.0 Bar
Focus	Active	Set Capillary	4500 V	Set Dry Heater	200 °C
Scan Begin	50 m/z	Set End Plate Offset	-500 V	Set Dry Gas	6.0 l/min
Scan End	3000 m/z	Set Charging Voltage	2000 V	Set Divert Valve	Waste
		Set Corona	0 nA	Set APCI Heater	0 °C

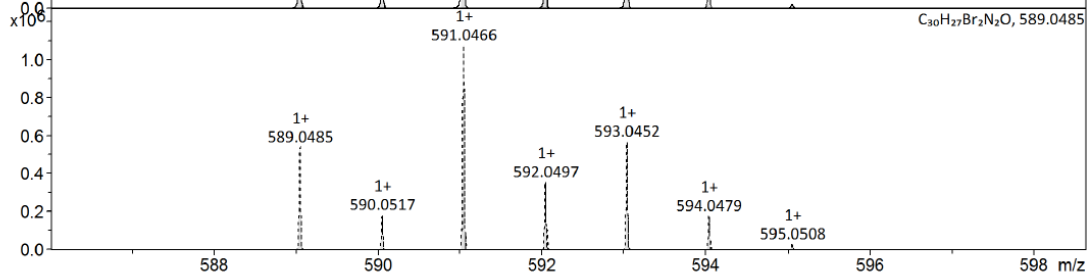
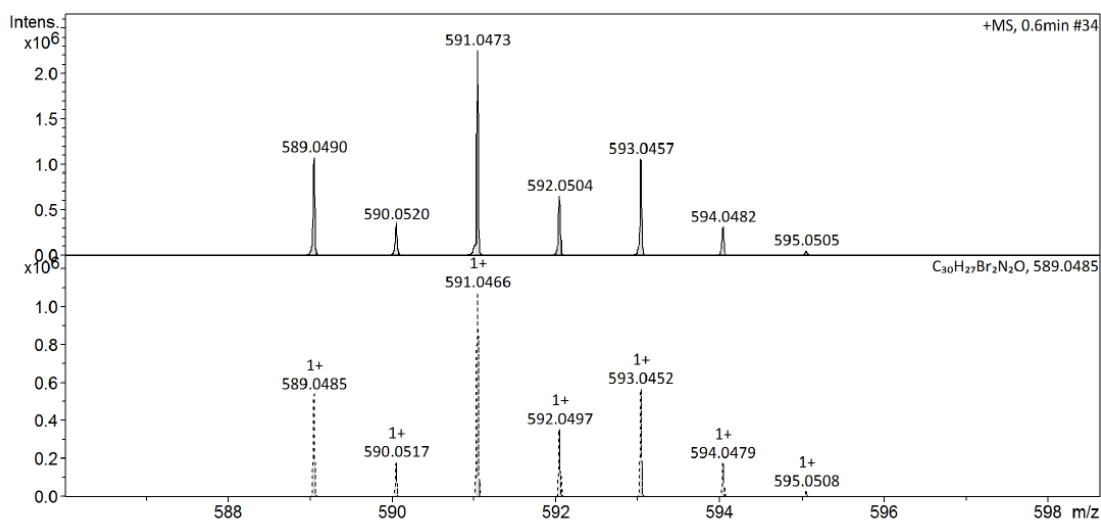
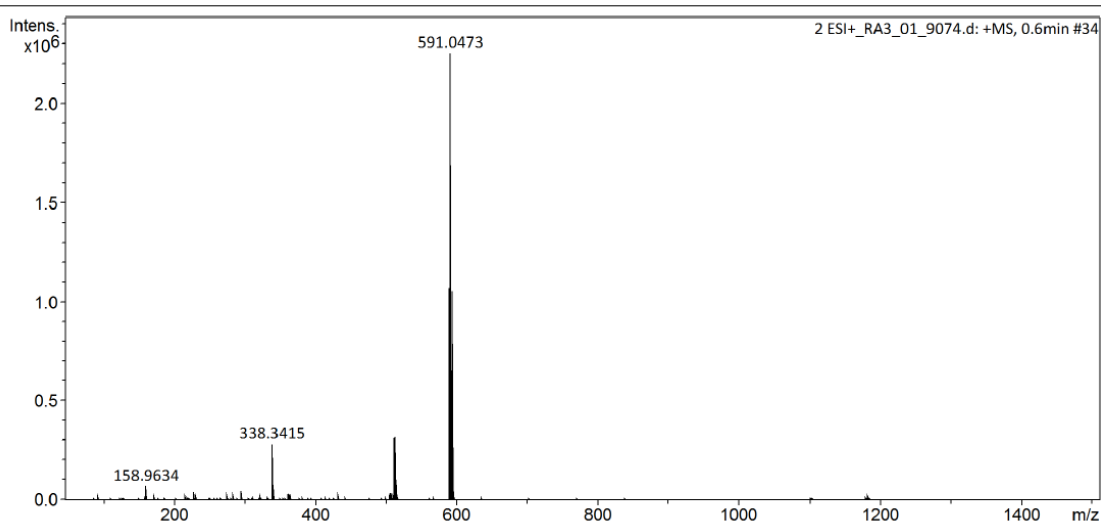


HRMS spectra of compound-2

Display Report

Analysis Info
Analysis Name D:\Data\nctu.service\data\2016\20160311\2 ESI+_RA3_01_9074.d
Method Small molecule.m
Sample Name 2 ESI+
Comment
Acquisition Date 3/11/2016 12:09:21 PM
Operator NCTU
Instrument impact HD 1819696.00164

Acquisition Parameter
Source Type ESI
Focus Active
Scan Begin 50 m/z
Scan End 1500 m/z
Ion Polarity Positive
Set Capillary 4500 V
Set End Plate Offset -500 V
Set Charging Voltage 2000 V
Set Corona 0 nA
Set Nebulizer 1.0 Bar
Set Dry Heater 200 °C
Set Dry Gas 6.0 l/min
Set Divert Valve Waste
Set APCI Heater 0 °C



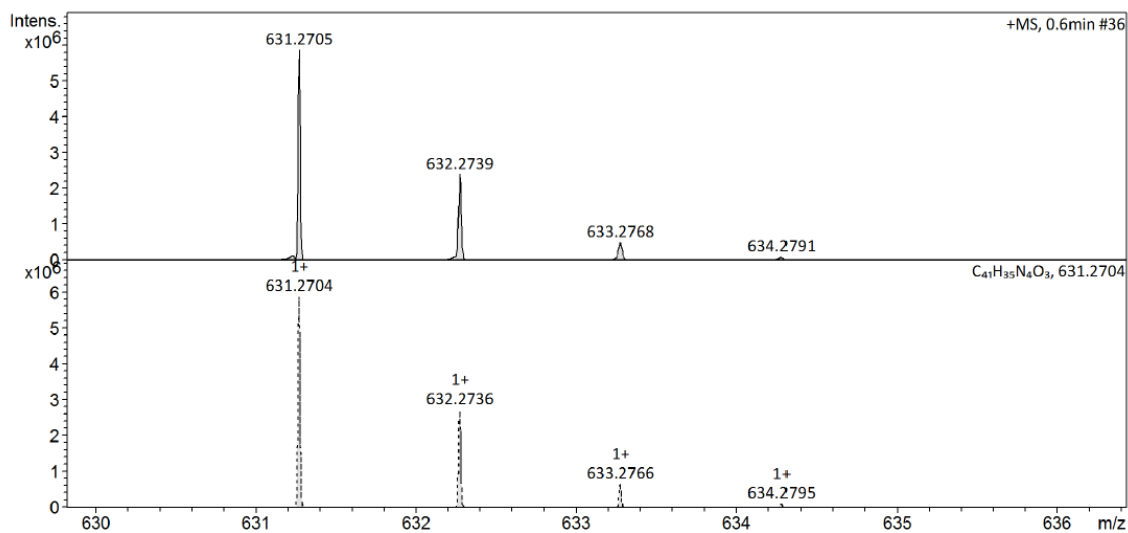
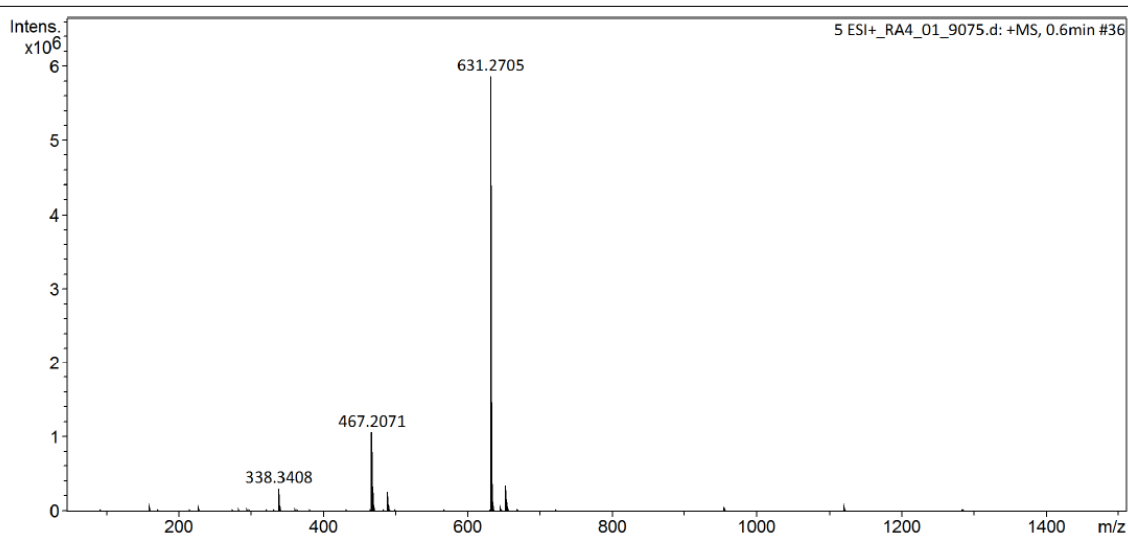
HRMS spectra of compound-5

Display Report

Analysis Info		Acquisition Date	3/11/2016 12:13:40 PM	
Analysis Name	D:\Data\ncu service\data\2016\20160311\5 ESI+_RA4_01_9075.d	Operator	NCTU	
Method	Small molecule.m	Instrument	impact HD	1819696.00164
Sample Name	5 ESI+			
Comment				

Acquisition Parameter

Source Type	ESI	Ion Polarity	Positive	Set Nebulizer	1.0 Bar
Focus	Active	Set Capillary	4500 V	Set Dry Heater	200 °C
Scan Begin	50 m/z	Set End Plate Offset	-500 V	Set Dry Gas	6.0 l/min
Scan End	1500 m/z	Set Charging Voltage	2000 V	Set Divert Valve	Waste
		Set Corona	0 nA	Set APCI Heater	0 °C

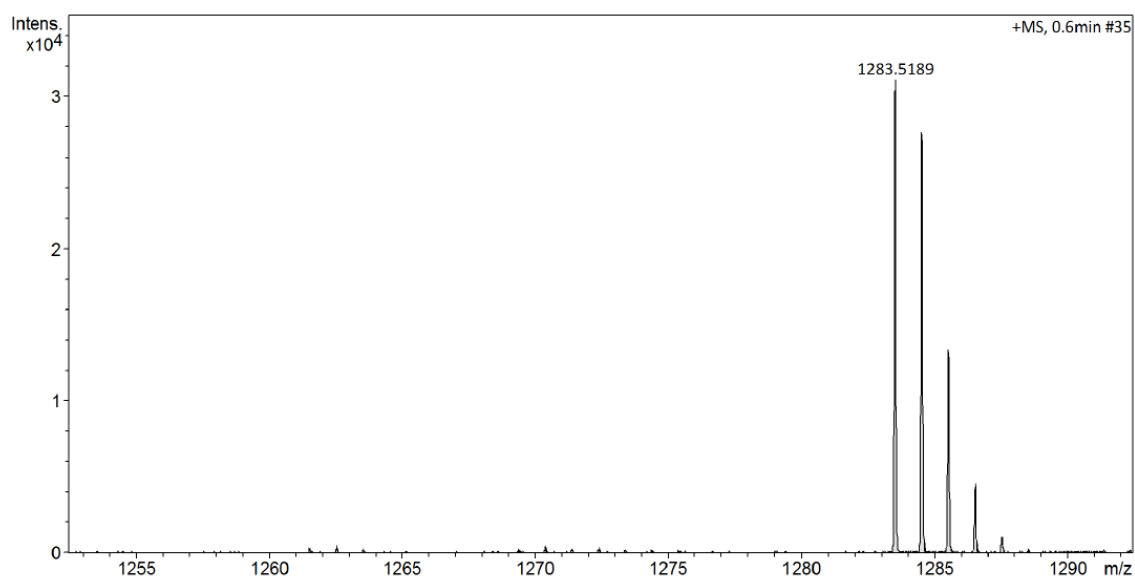
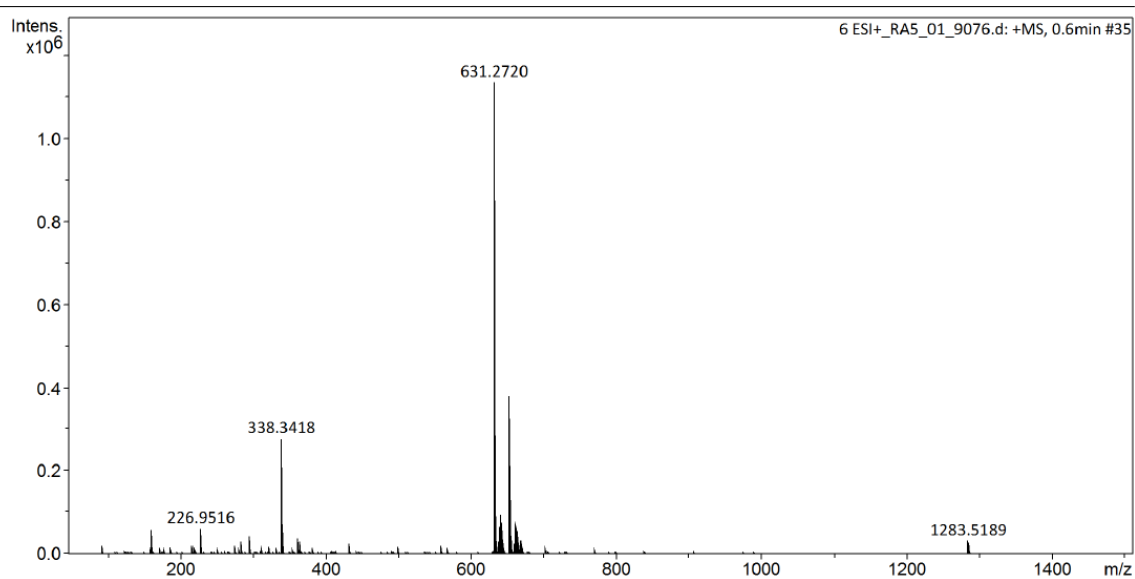


HRMS spectra of compound-6

Display Report

Analysis Info		Acquisition Date	3/11/2016 12:17:56 PM	
Analysis Name	D:\Data\nctu service\data\2016\20160311\6 ESI+_RA5_01_9076.d	Operator	NCTU	
Method	Small molecule.m	Instrument	impact HD	1819696.00164
Sample Name	6 ESI+	Comment		

Acquisition Parameter					
Source Type	ESI	Ion Polarity	Positive	Set Nebulizer	1.0 Bar
Focus	Active	Set Capillary	4500 V	Set Dry Heater	200 °C
Scan Begin	50 m/z	Set End Plate Offset	-500 V	Set Dry Gas	6.0 l/min
Scan End	1500 m/z	Set Charging Voltage	2000 V	Set Divert Valve	Waste
		Set Corona	0 nA	Set APCI Heater	0 °C



HRMS spectra of compound-7

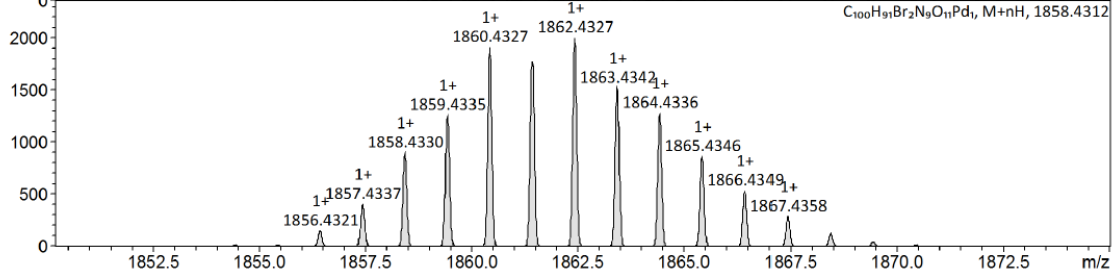
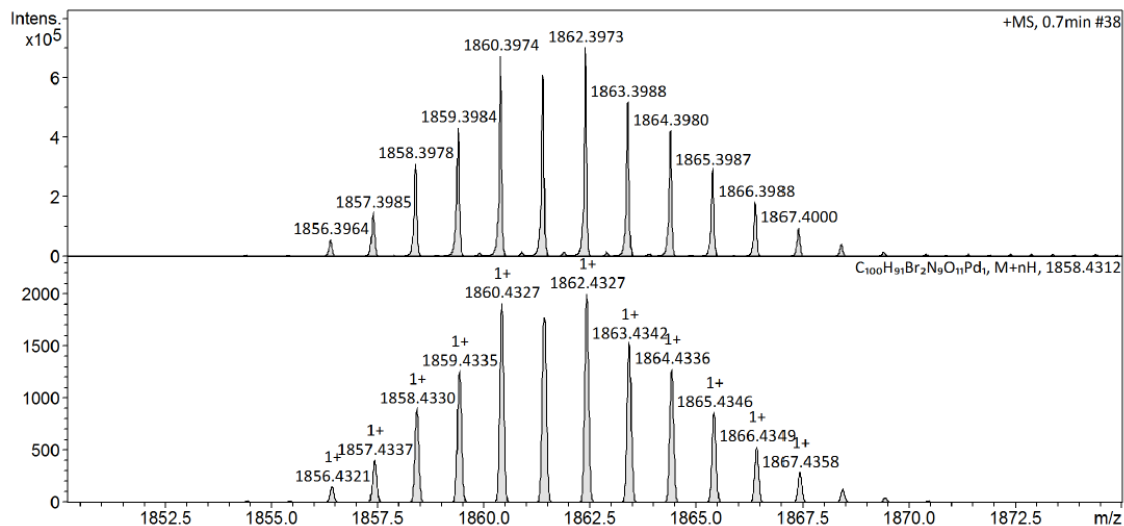
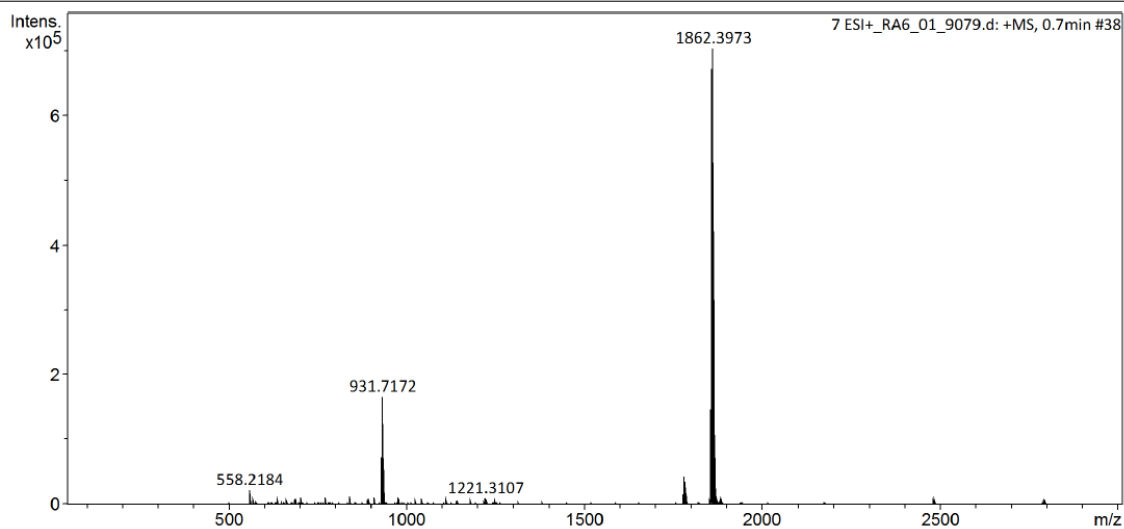
Display Report

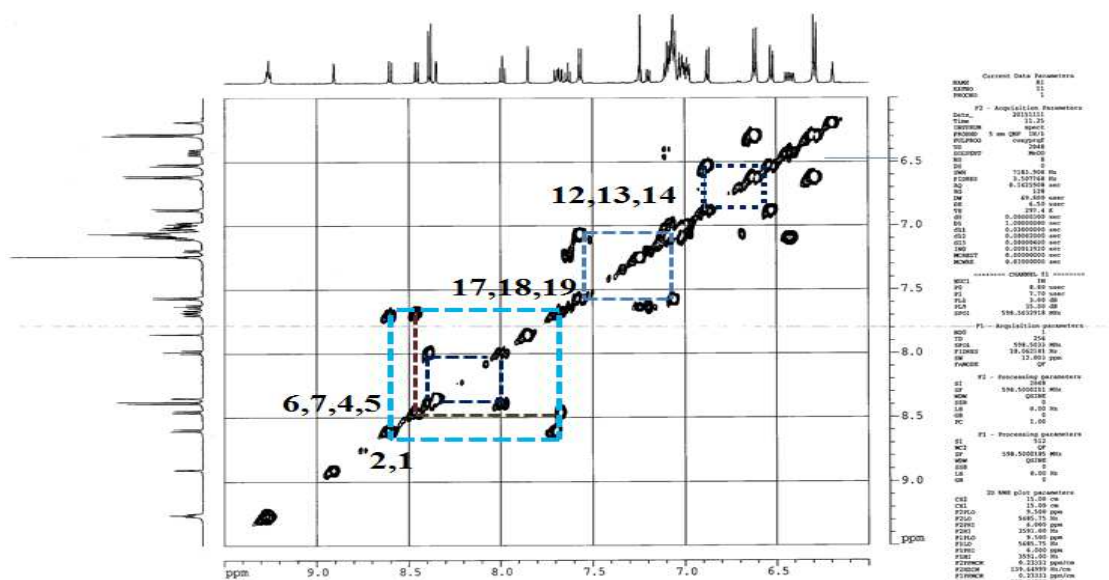
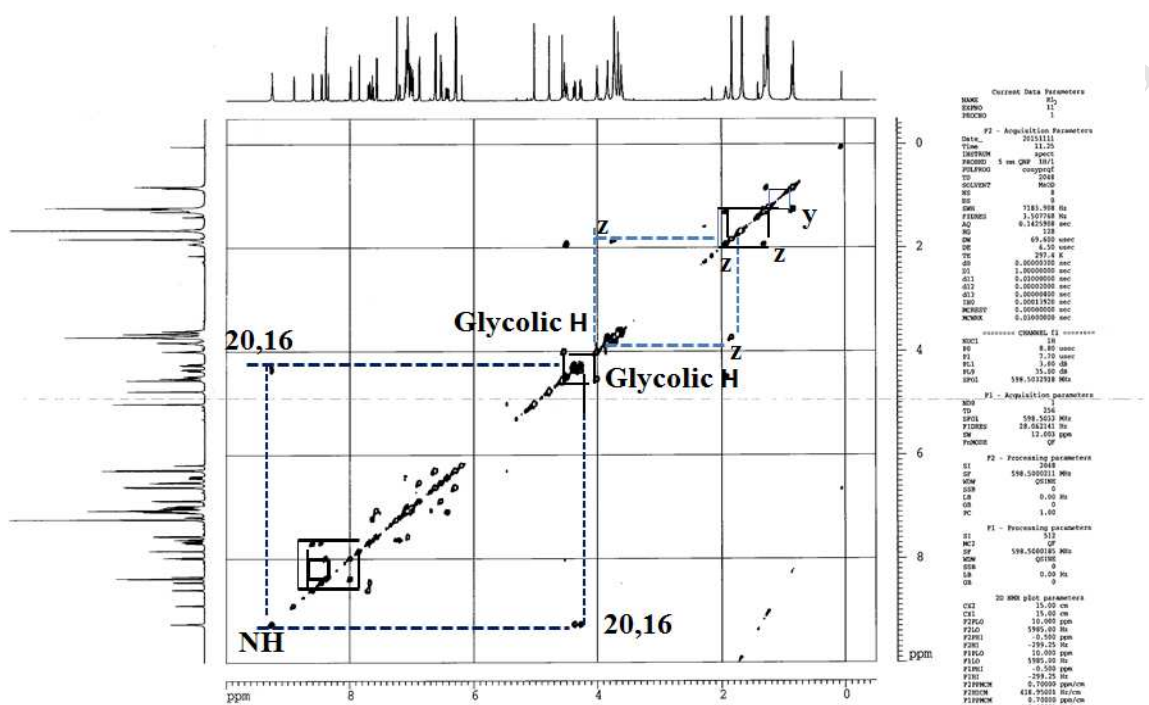
Analysis Info

Analysis Name	D:\Data\ntcu service\data\2016\20160311\7 ESI+_RA6_01_9079.d	Acquisition Date	3/11/2016 12:30:43 PM	
Method	MW600-3000.m	Operator	NCTU	
Sample Name	7 ESI+	Instrument	impact HD	1819696.00164
Comment				

Acquisition Parameter

Source Type	ESI	Ion Polarity	Positive	Set Nebulizer	1.0 Bar
Focus	Active	Set Capillary	4500 V	Set Dry Heater	200 °C
Scan Begin	50 m/z	Set End Plate Offset	-500 V	Set Dry Gas	6.0 l/min
Scan End	3000 m/z	Set Charging Voltage	2000 V	Set Divert Valve	Waste
		Set Corona	0 nA	Set APCI Heater	0 °C



2D ^1H - ^1H COSY NMR spectrum of rotaxane R1 in CDCl_3 

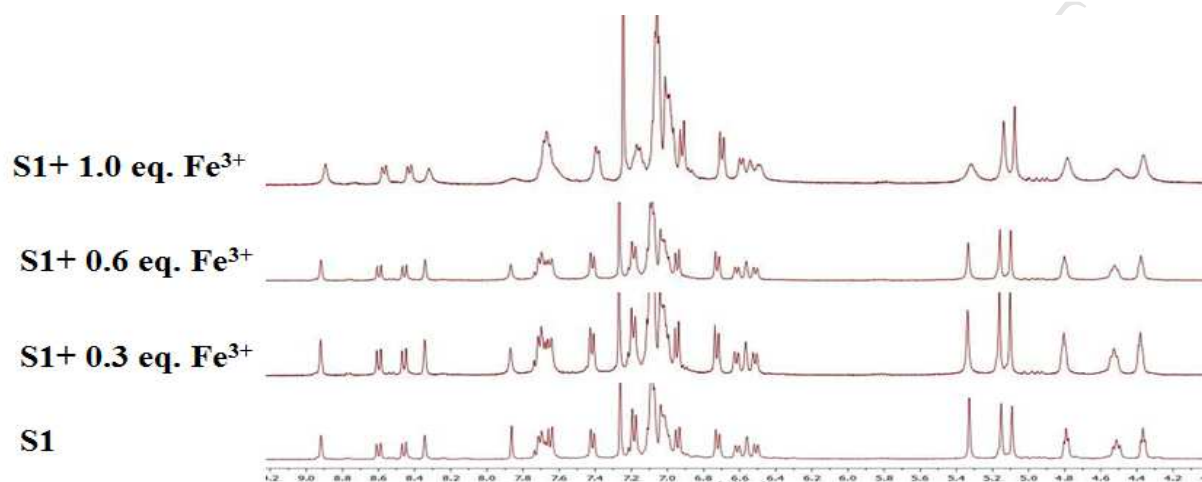


Figure S1. ^1H -NMR titration spectra of axle **S1** in CDCl_3 with the increment of Fe^{3+} metal ion.

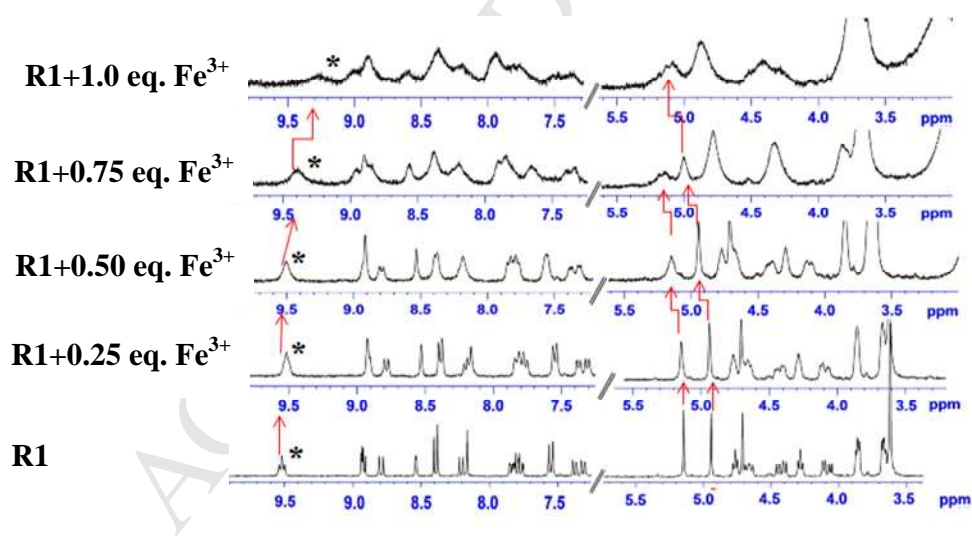


Figure S2. ^1H -NMR titration spectra of **R1** in $\text{acetone-}d_6$ with the increment of Fe^{3+} metal ion.

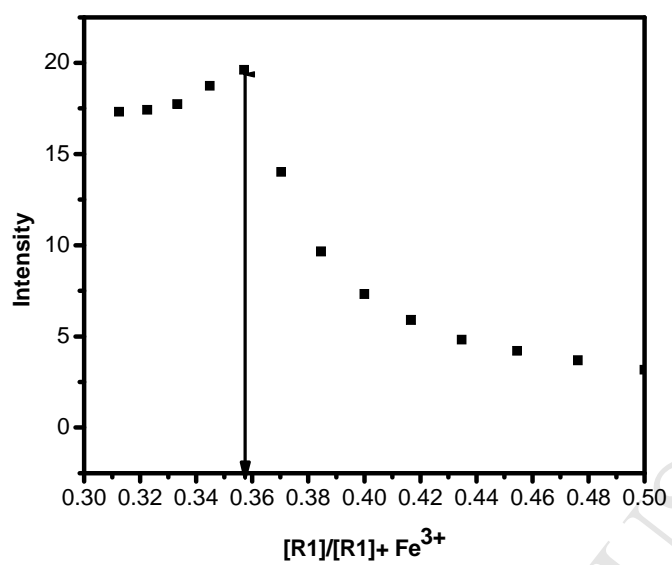


Figure S3. Job's plot of **R1** indicating a 1:1 stoichiometry between **R1** and Fe³⁺. (*Org. Biomol. Chem.*, 2013,

11, 765–772)

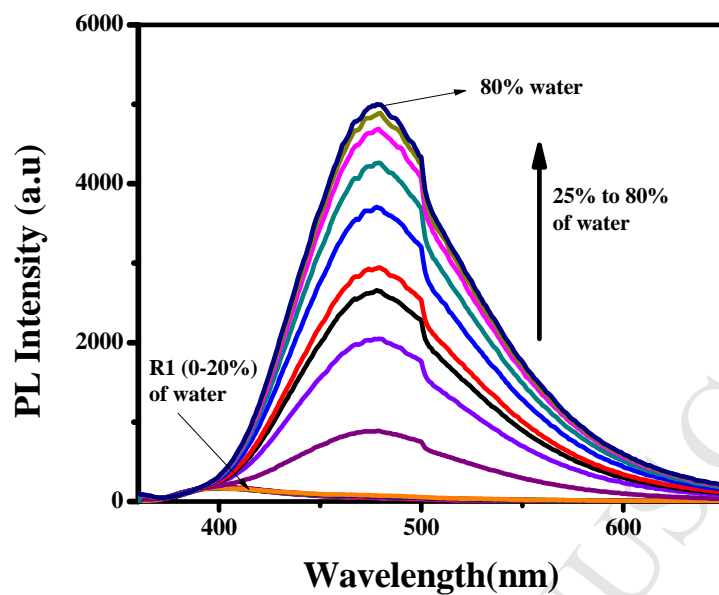


Figure S4. PL spectra of **R1** with increasing water fraction (from 25% to 80%).

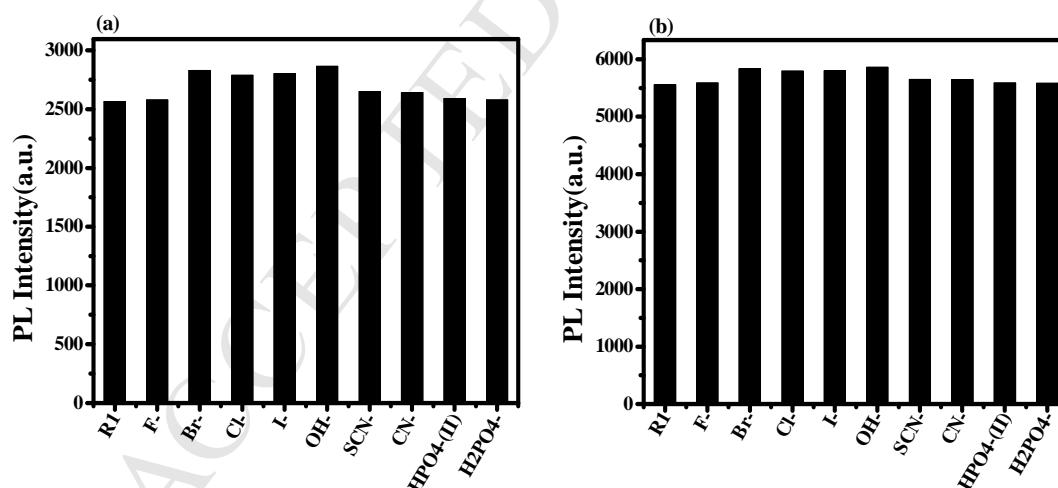


Figure S5. (a) Bar diagrams depicting PL intensities of **R1** towards various anions (a) 10 % and (b) 80% aq., HEPES (pH 7.4, 10 mM) in DMSO with various anions.

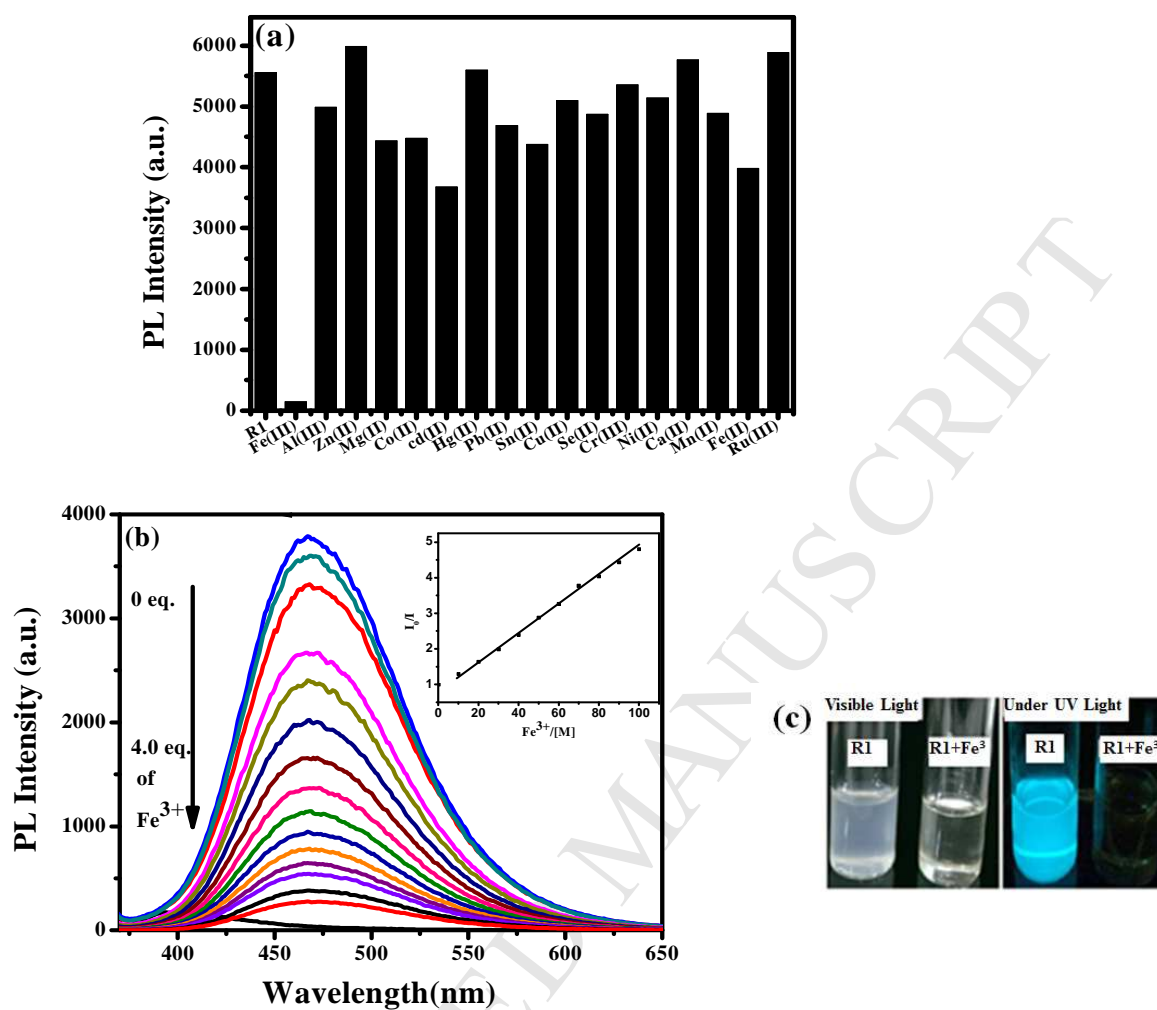


Figure S6. (a) Bar diagrams depicting PL quantities of **R1**+ Fe³⁺ in 80% aq., HEPES (pH 7.4, 10 mM) in DMSO with various metal ions. (b) PL quenching of **R1** (25 μ M) in 80% of aq., in above solution with increasing concentrations of Fe³⁺ ion. (c) Color changes of **R1** visible light and under UV light in above solution.

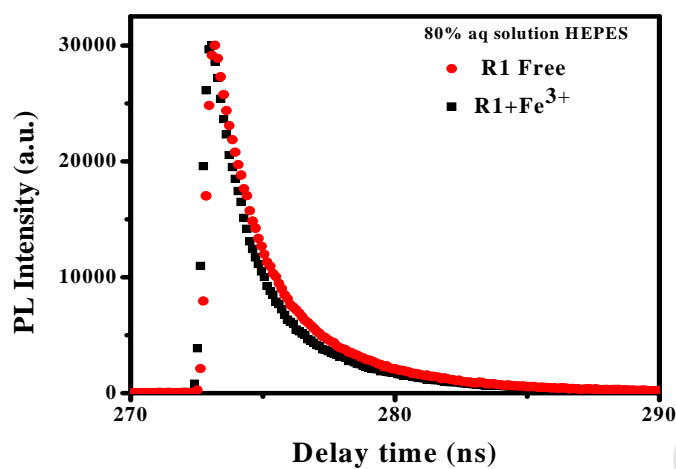


Figure S7. Decay patterns of **R1** in the presence of Fe³⁺ ion in 80% of aq. (aggregated state), HEPES pH 7.4, 10 mM in DMSO.

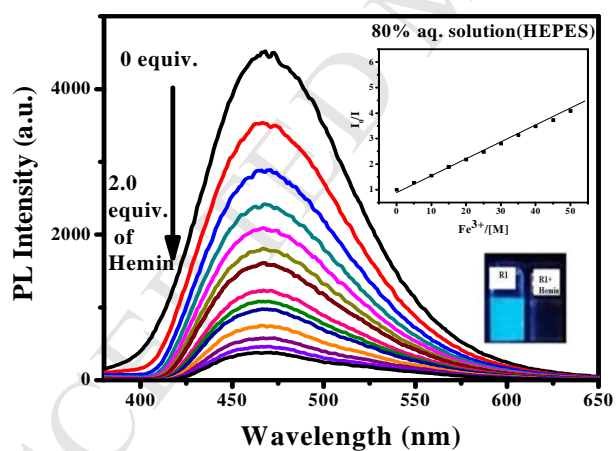


Figure S8. PL titration spectra of **R1** (25 μM) with Hemin (50 μM) in 80% of aq. (aggregated state), HEPES pH 7.4, 10 mM in DMSO.

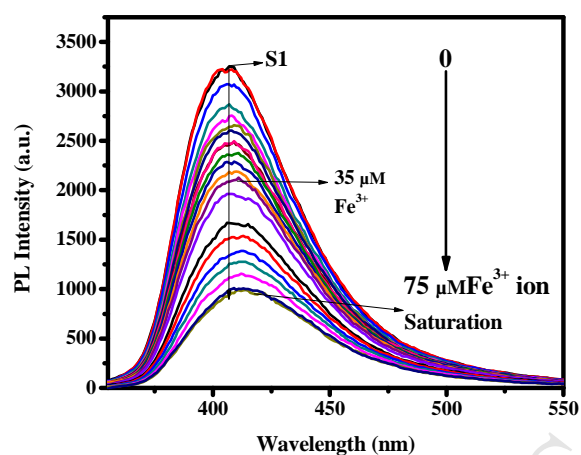


Figure S9. PL titration spectra of **S1** (25 μM) with Fe^{3+} (0-75 μM) in 10% of aq., HEPES pH 7.4, 10 mM in DMSO.

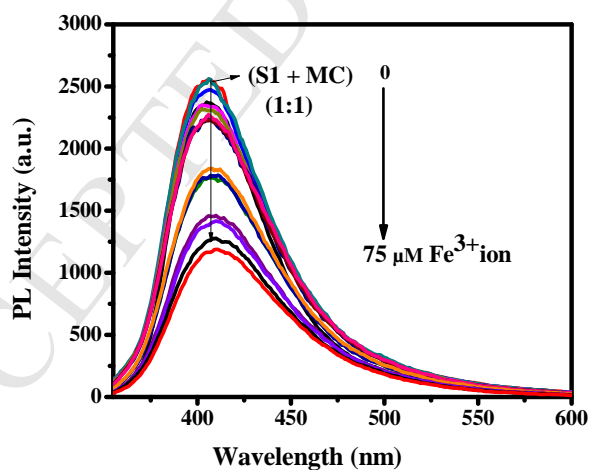


Figure S10. PL titration spectra of the combination of **S1** (25 μM) + macro-cycle **MC** (25 μM) in a molar ratio of 1:1 with Fe^{3+} (0-75 μM) in 10% of aq., HEPES pH 7.4, 10 mM in DMSO.

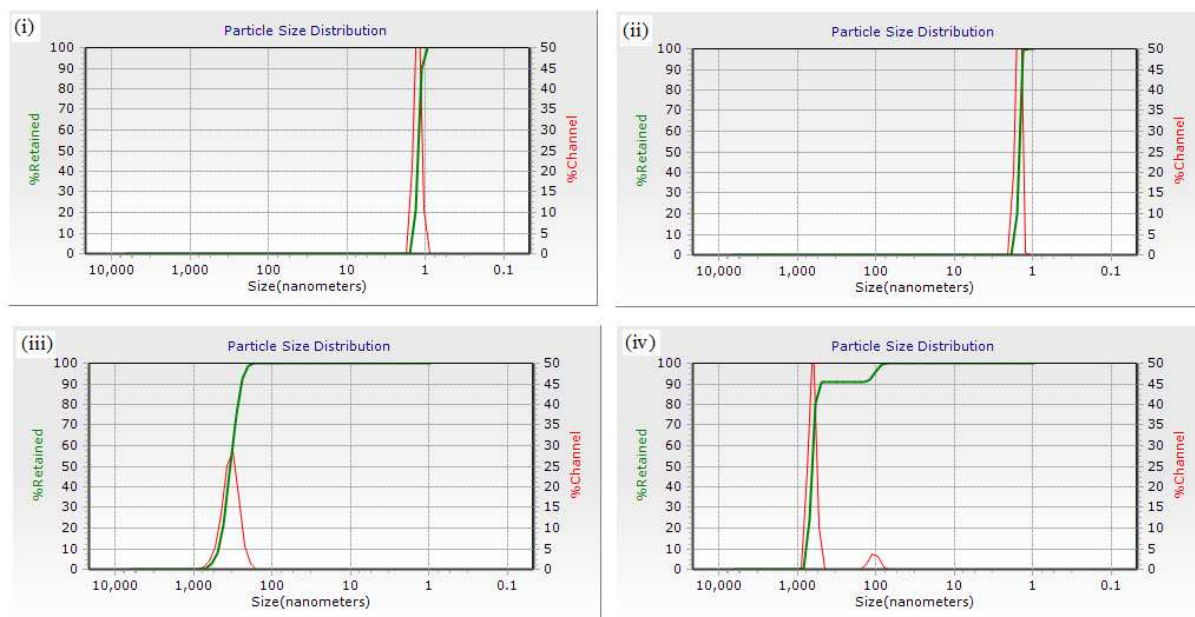


Figure S11. DLS measurements of particle sizes for (i) **R1** and (ii) **R1** + Fe^{3+} , (iii) **R1**_{aggregate} and (iv) **R1**_{aggregate} + Fe^{3+} .

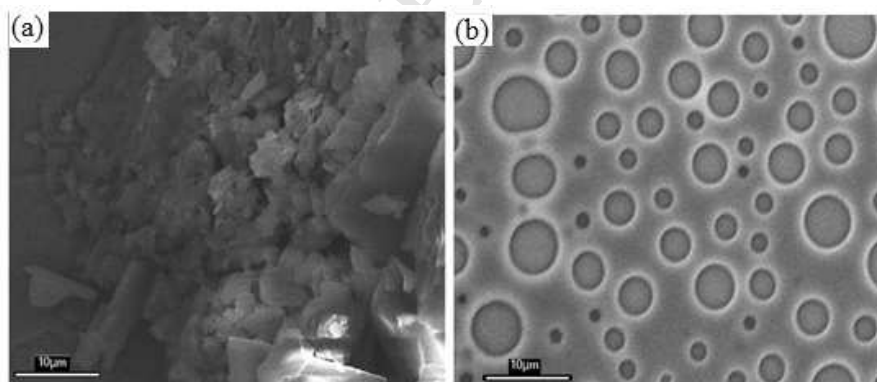


Figure S12. SEM images of (a) **R1** free and (b) **R1** in the presence of Fe^{3+} metal ion (1:1).

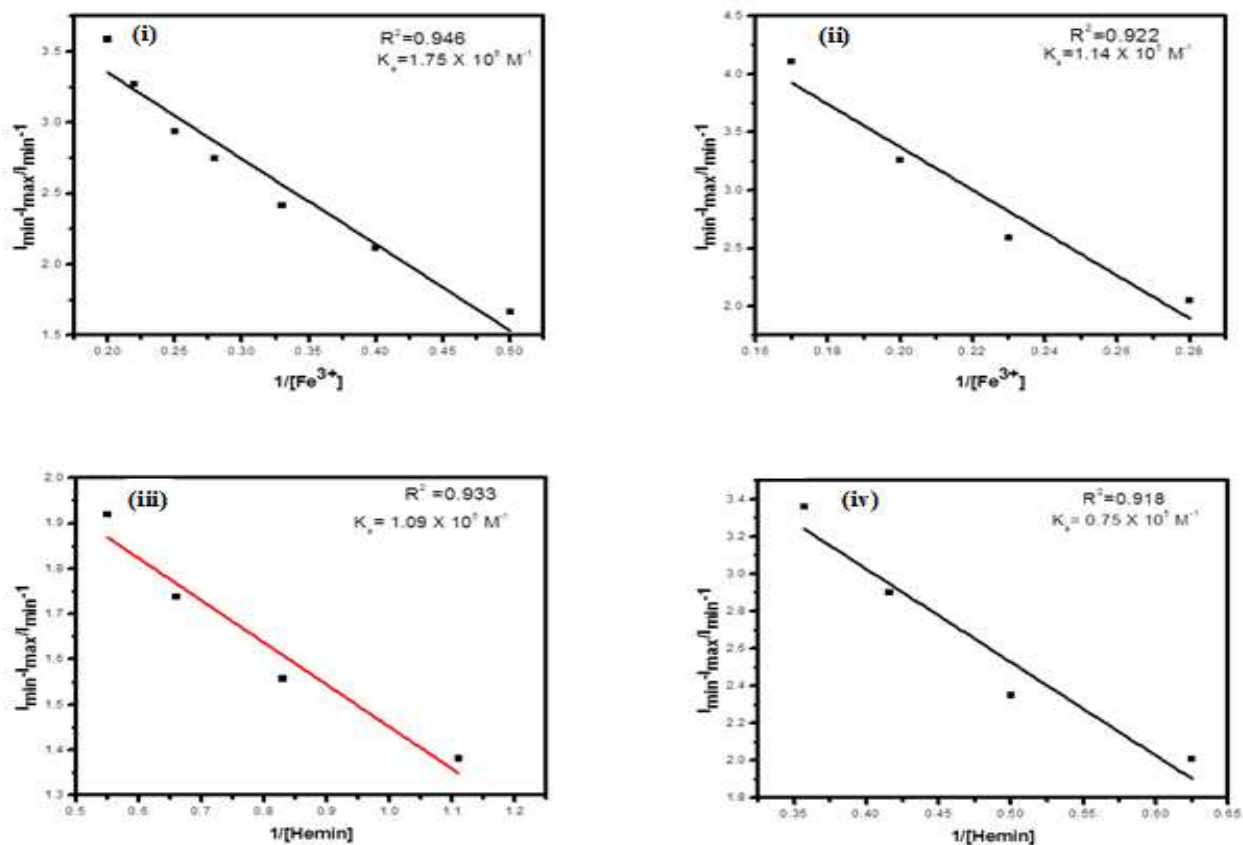


Figure S13. Binding constant plot (connor method) of R1 with Fe^{3+} (i) and (ii) and with Hemin (iii) and (iv) in the non-aggregated (10 % aq.) and aggregated (80 % aq.) states, respectively.

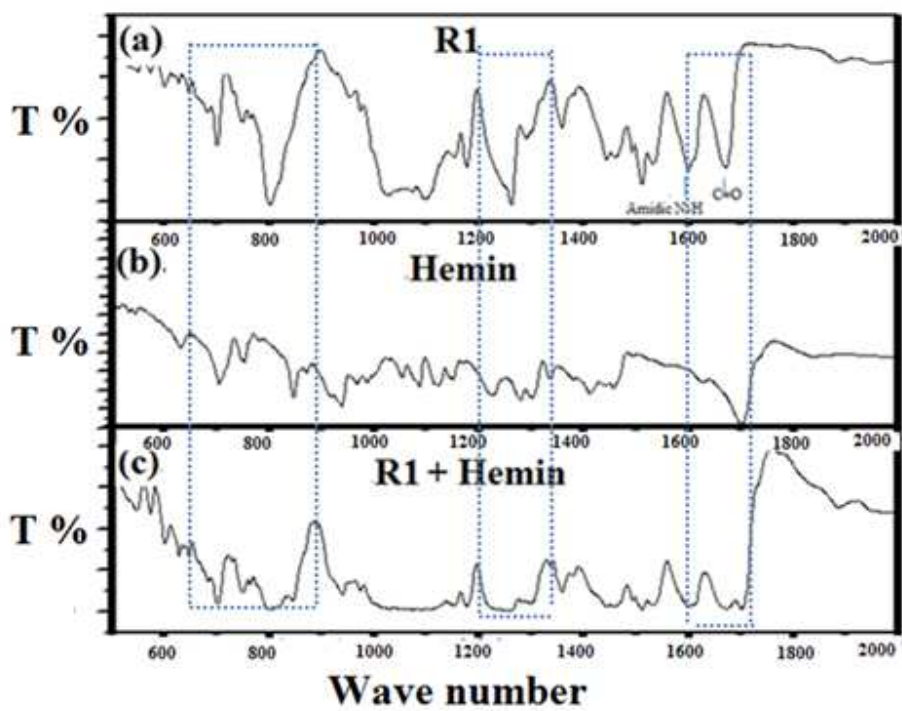
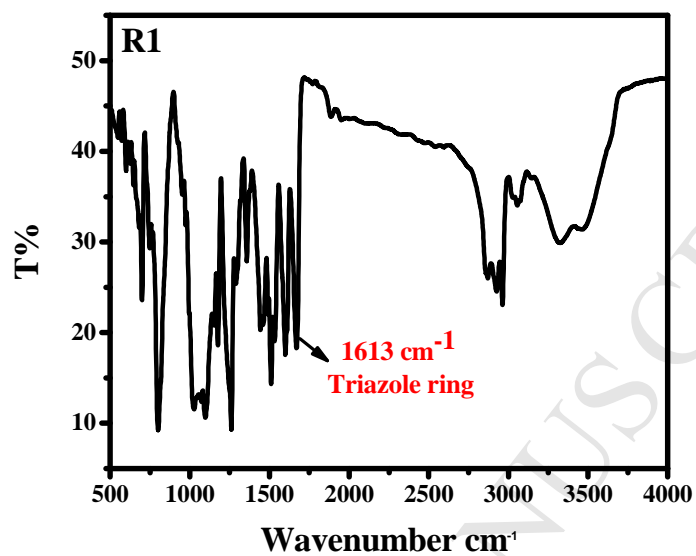


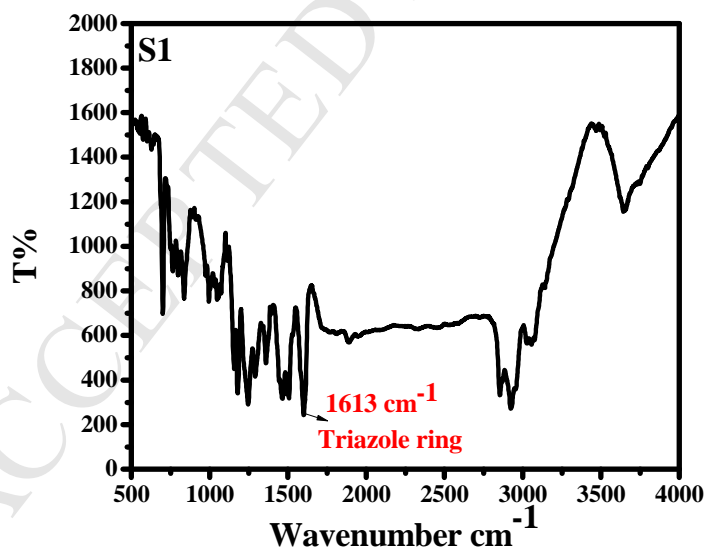
Figure S13. FTIR of (a) **R1** (b) Hemin (c) **R1+Hemin**, (1/1) recorded in KBr matrix.

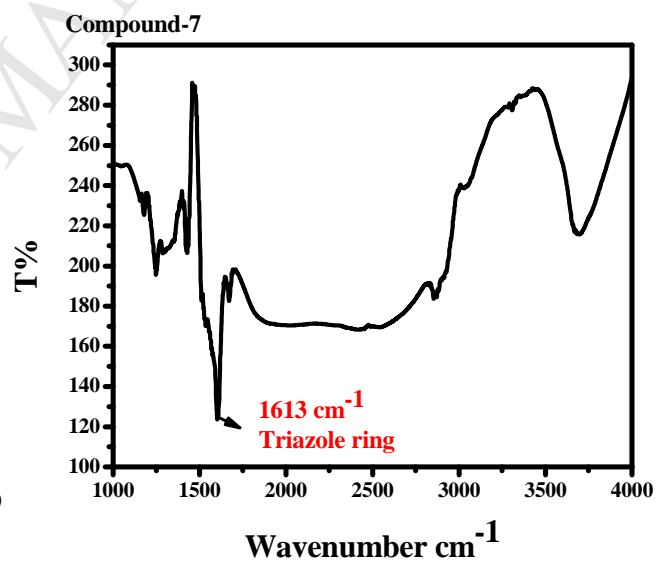
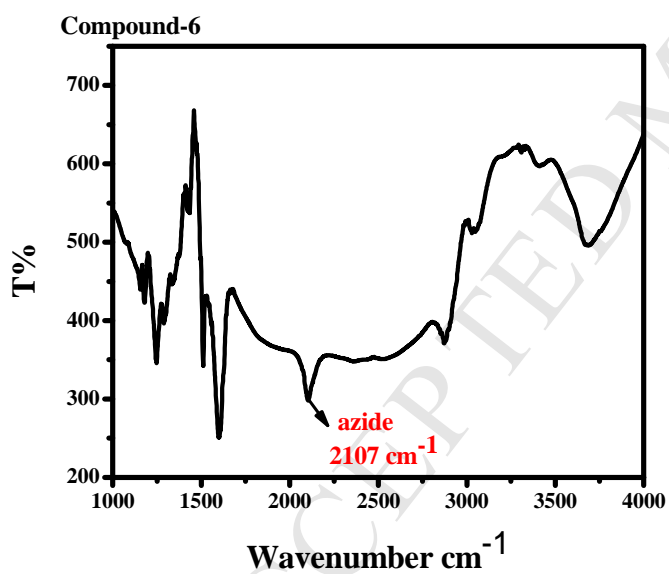
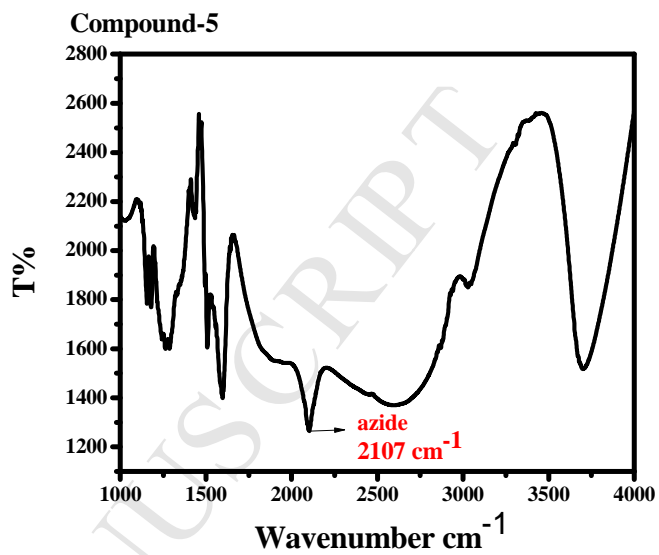
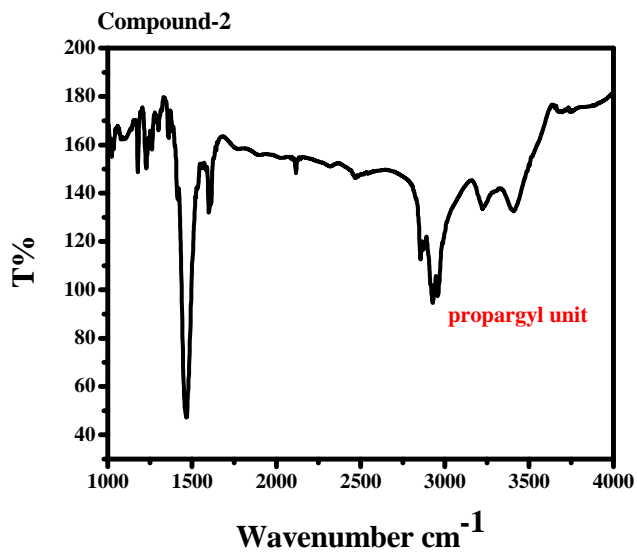
FTIR spectra :

Rotaxane R1

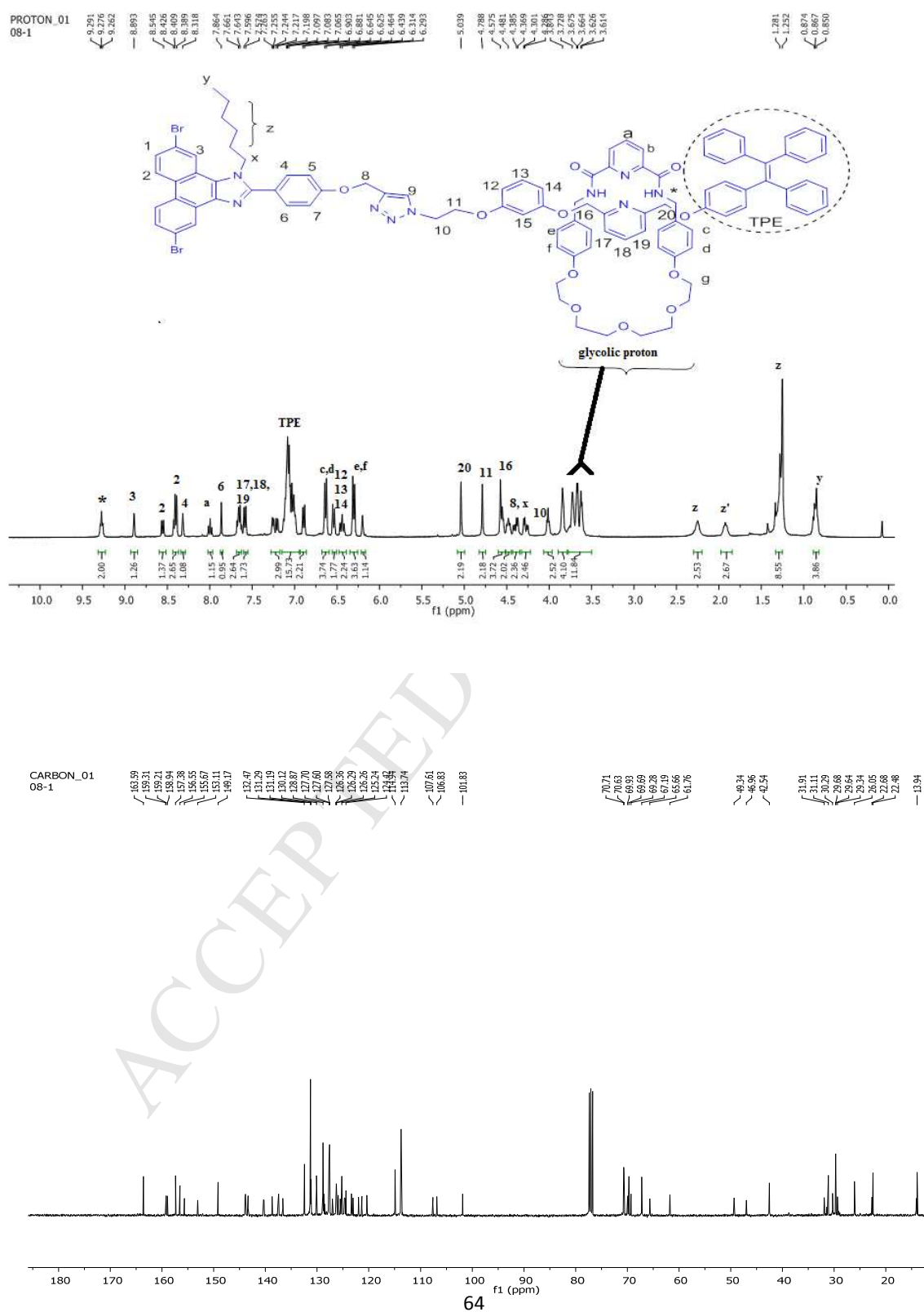


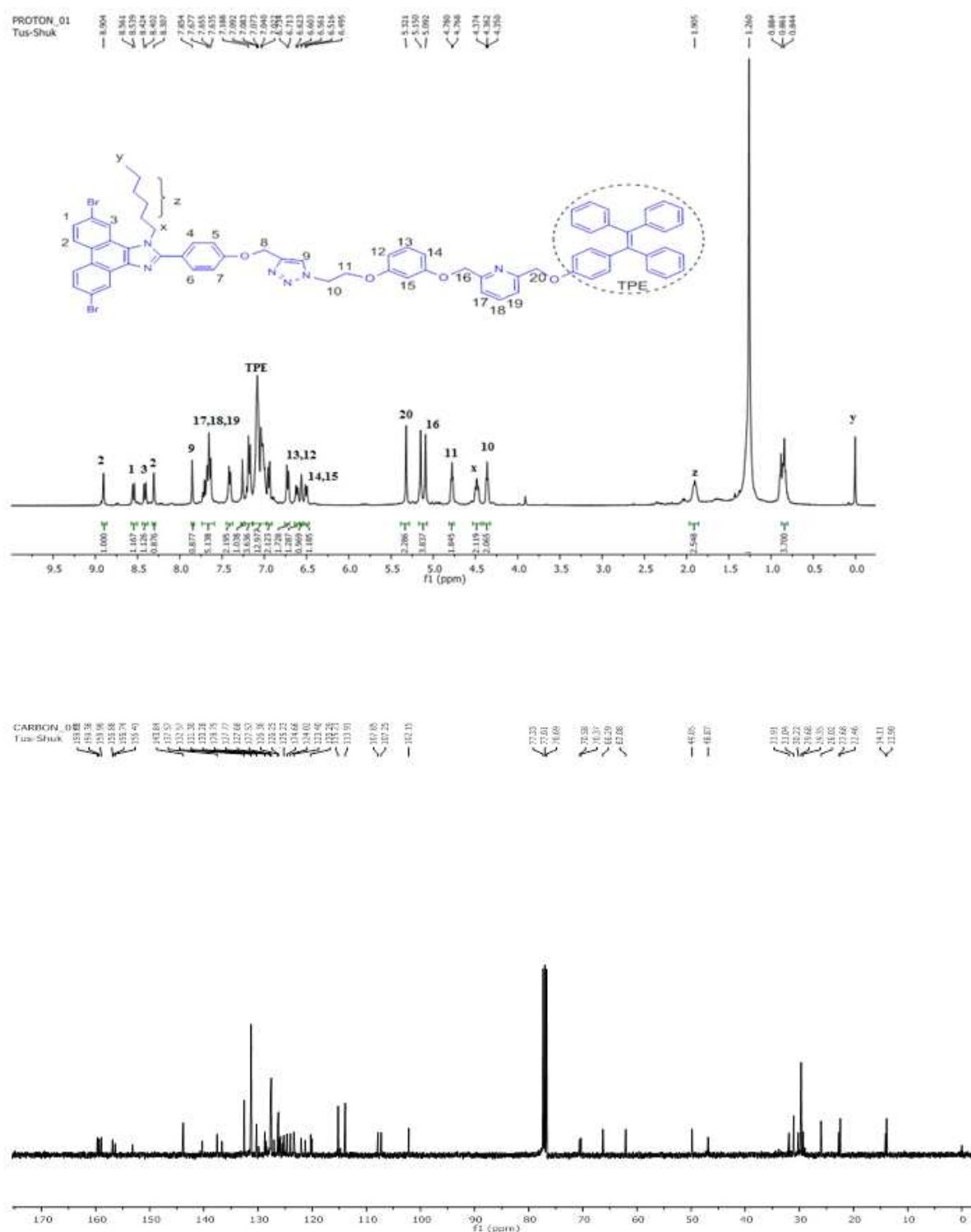
Stopper S1 :

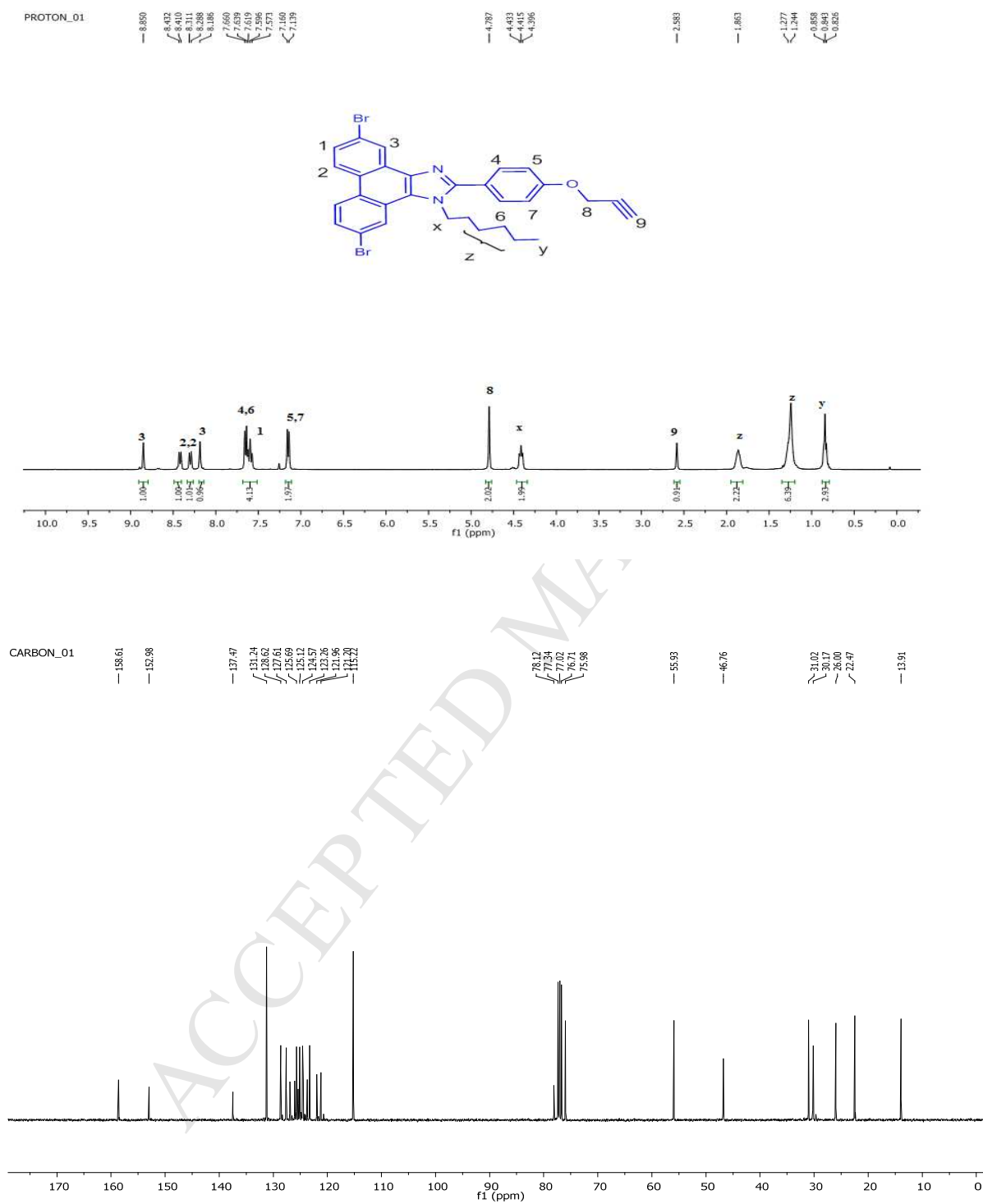




1H NMR and 13C NMR spectra of R1

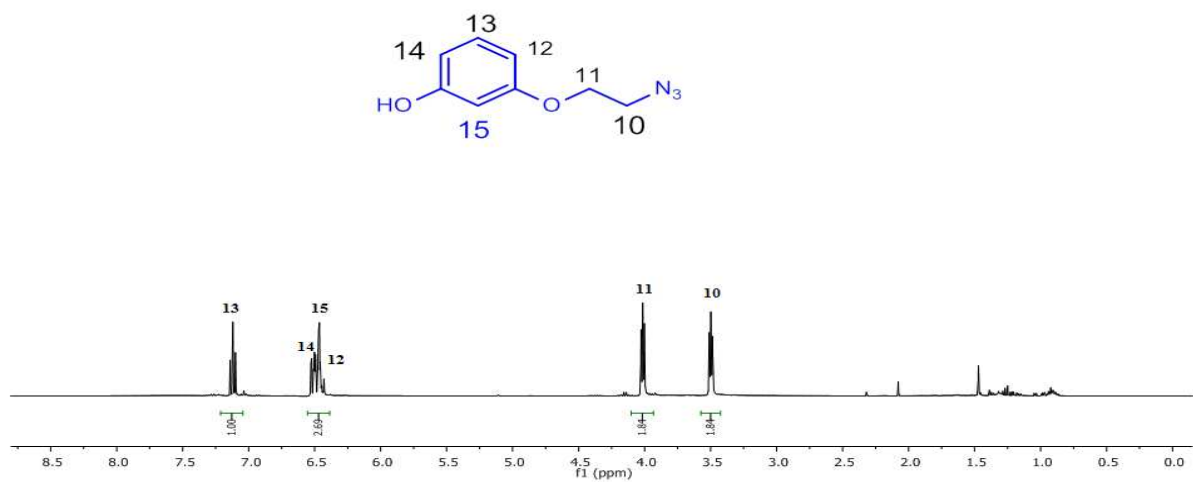


¹H NMR and ¹³C NMR spectra of axle S1

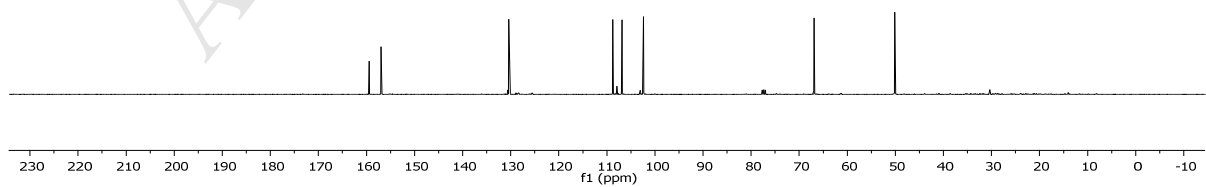
¹H NMR and ¹³C NMR spectra of compound 2

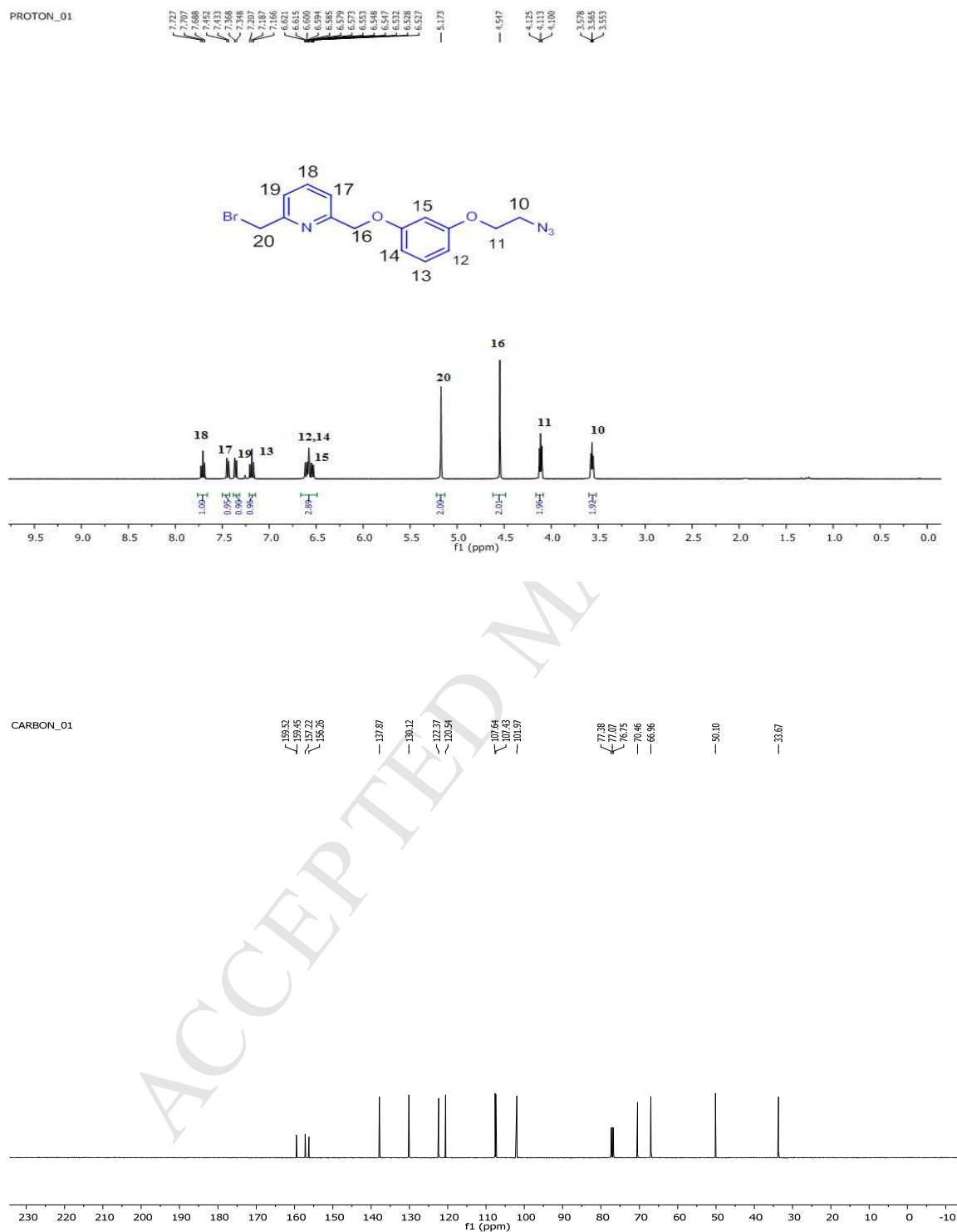
¹H NMR and ¹³C NMR spectra of compound 3

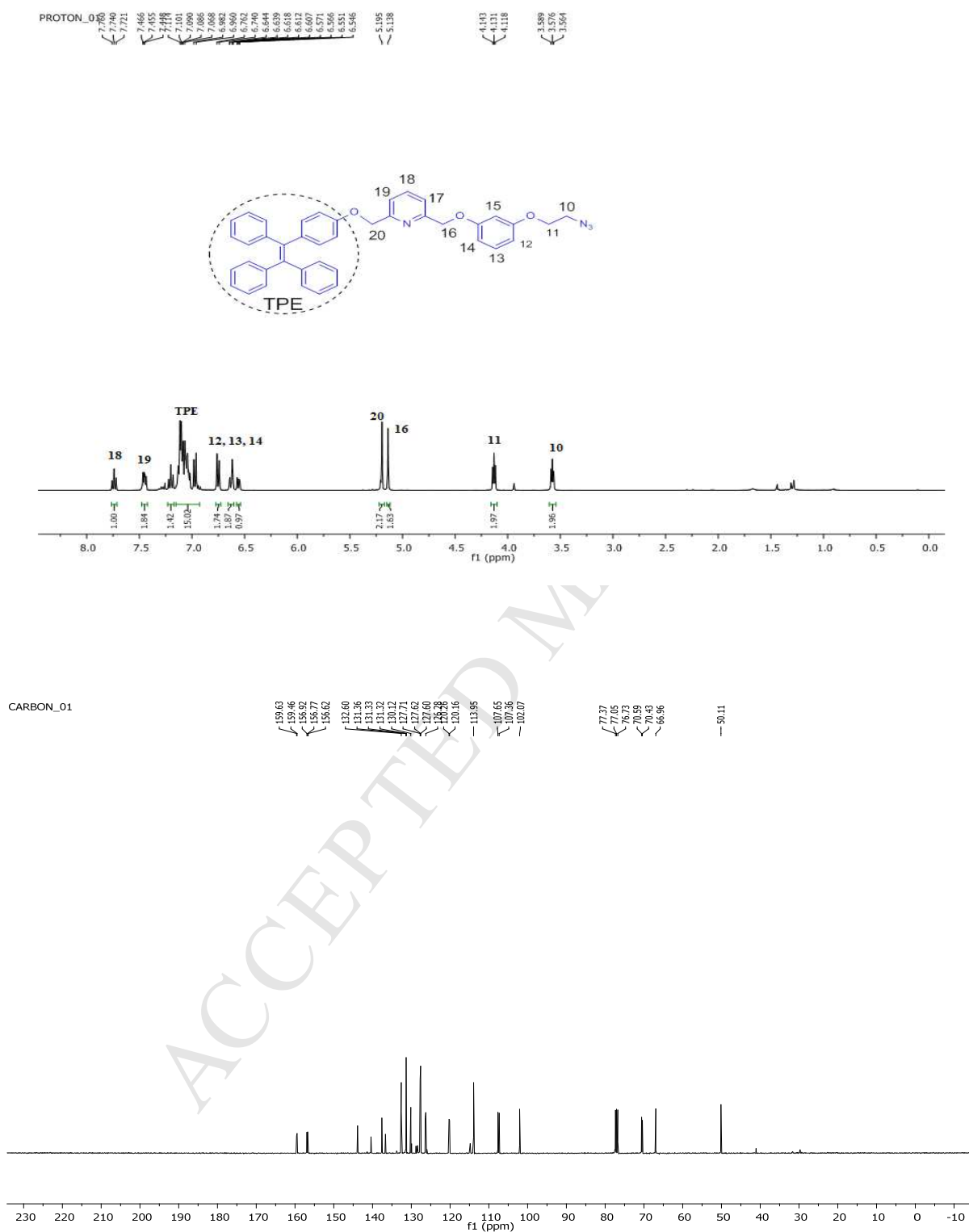
PROTON_01

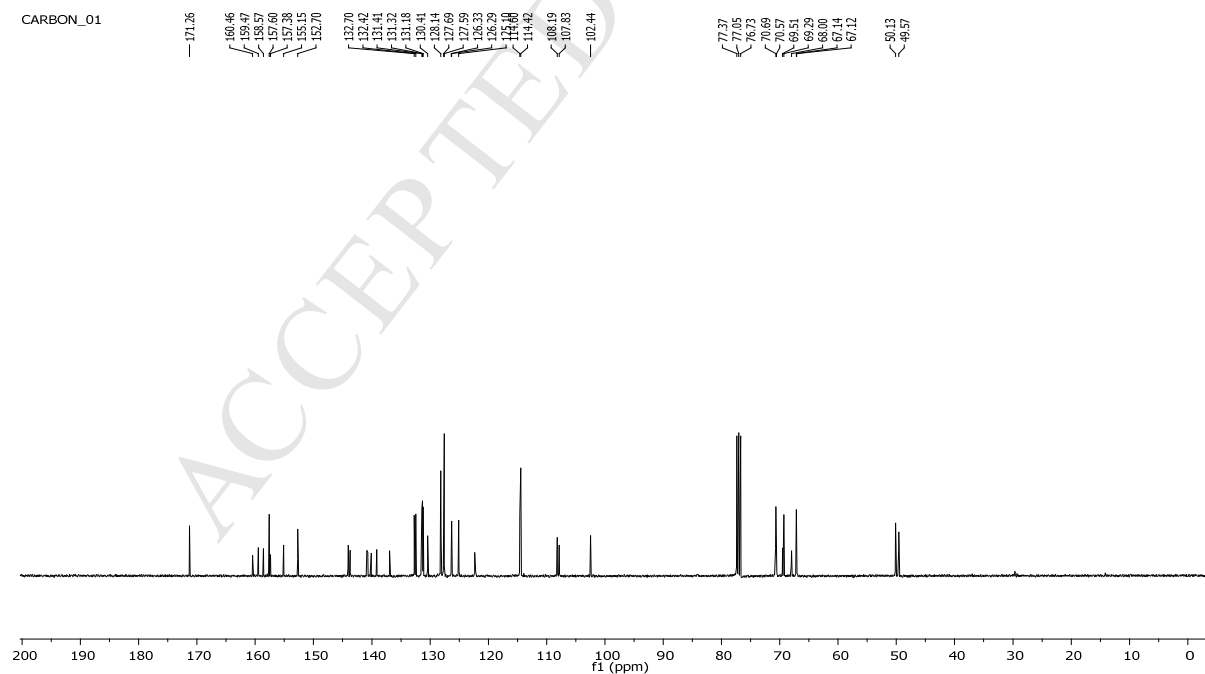
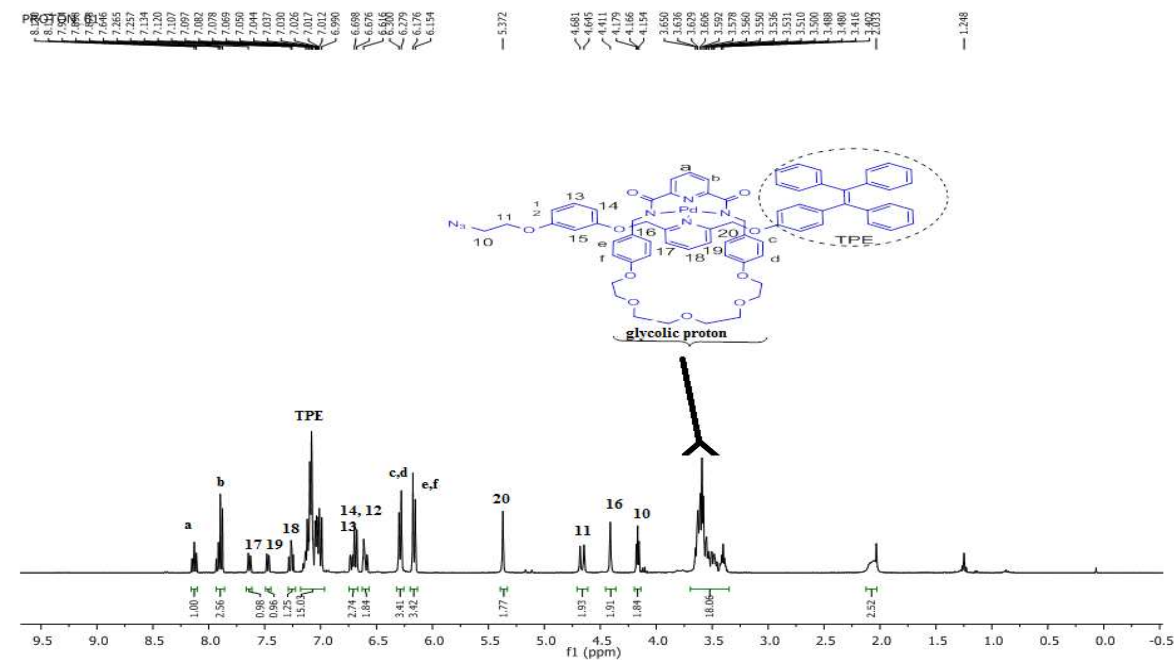


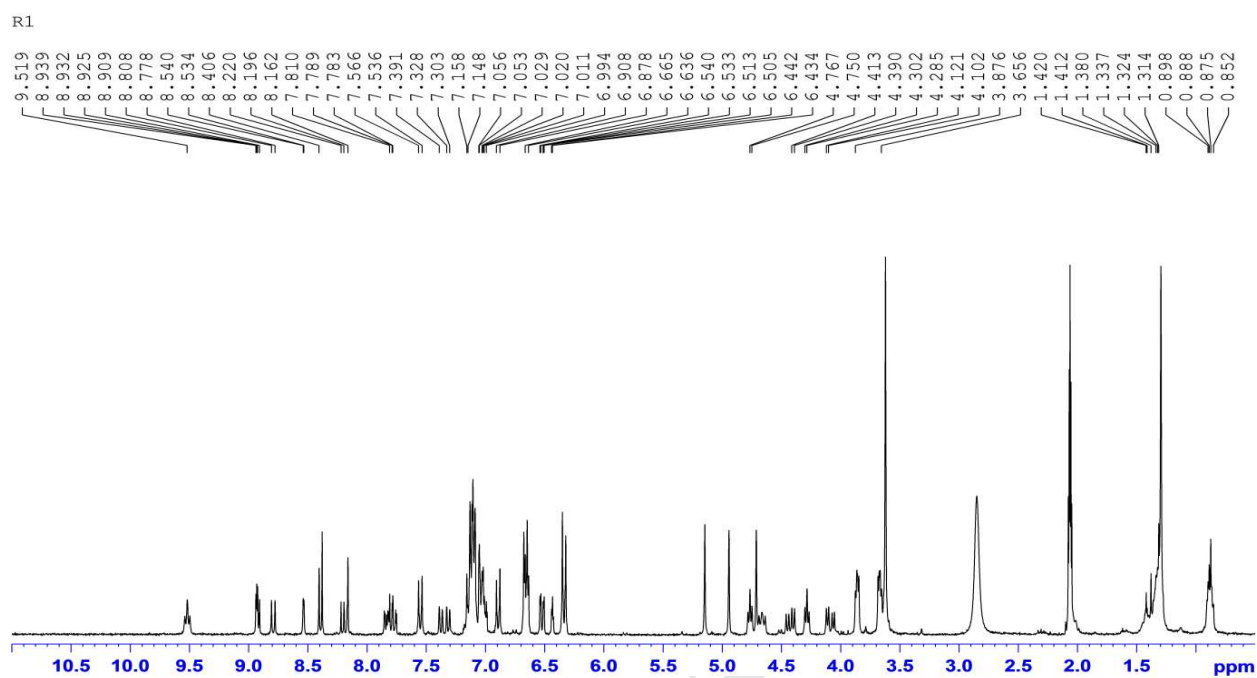
CARBON_01



¹H NMR and ¹³C NMR spectra of compound 4

¹H NMR and ¹³C NMR spectra of compound 5

¹H NMR and ¹³C NMR spectra of compound 6

¹H NMR spectra of R1 in Acetone (d₆)**¹H NMR spectra of R1 in DMSO (d₆)**